



Channel Estimation and Equalization for Alamouti SF-Coded OFDM-UWA Communications

Erdal Panayirci , *Life Fellow, IEEE*, Mhd Tahssin Altabbaa , *Member, IEEE*,
and H. Vincent Poor , *Life Fellow, IEEE*

Abstract—In this paper, a new channel estimation and equalization algorithm for underwater acoustic (UWA) communications is presented. The proposed algorithm is developed to meet the requirements of underwater time-varying sparse channels that undergo Rayleigh fading. In addition, the algorithm takes into consideration a path-based channel model which describes each received path with significant power by an attenuation factor, a Doppler scale, and a delay. Transmit diversity enabled by Alamouti space-frequency block coding coupled with orthogonal frequency division multiplexing is employed in the form of two transmitters and multiple receivers. The proposed, non-data-aided, expectation-maximization (EM)-based maximum *a posteriori* probability sparse channel estimation first estimates the channel transfer functions from each transmit antenna to the receiver. Then, the estimation performance is greatly improved by taking into account the sparseness of the UWA channel and refining the estimation based on the sparse solution that best matches the frequency-domain channel estimates obtained during the first phase of the estimation process. Sparse channel path delays and Doppler scaling factors are estimated by a novel technique called *delay focusing*. After that, slow time-varying, complex-valued channel path gains are estimated using a basis expansion model based on the discrete Legendre polynomial expansion. Computer simulation results show that the resulting channel estimation algorithm can achieve excellent mean-square error and symbol error rate for both generated data and semi-experimental data taken at Sapanca Lake in Turkey and is capable of handling some mismatch due to different fading models.

Index Terms—Alamouti space-frequency block code, basis expansion model, Delay focusing, MAP-EM channel estimation, underwater acoustic communications.

I. INTRODUCTION

COMMUNICATION over underwater wireless channels has been applied using acoustic waves. In underwater

environments, acoustic waves experience lower attenuation than electromagnetic waves and lower scattering than light waves experience in such environment [1]. However, the time-varying sparse acoustic channels have larger delays and Doppler shifts. This is due to the relatively low speed of acoustic waves and the transceiver motion, respectively. In addition, the placement of the transceiver pair in underwater environments is affected by different fading phenomena. That is, it has been shown experimentally that when the transceiver pair are in shallow-water, the underwater channel gains experience Rician fading. Whereas, in deep water-based systems, a Rayleigh type of channel fading is encountered [2].

Terrestrial wireless technologies for channel transfer function estimation, equalization, and data detection have been applied to underwater acoustic communications (UWACs). In particular, studies described in the literature exploit the sparse nature of underwater acoustic (UWA) channels [3]–[5]. In addition, employing multi-carrier transmission, such as orthogonal frequency division multiplexing (OFDM) has shown robustness against underwater inter-symbol interference (ISI). Several methods and techniques have been proposed for estimating the channel path gains and their corresponding delays in the presence of large Doppler spreads and for their compensation to mitigate the impairments arising in UWACs [6]. Compressed sensing approaches, such as the matching pursuit (MP) algorithm, have been shown to be effective in estimating the UWAC channel parameters [7], [8]. Notably, modified versions of the MP algorithm, such as orthogonal-MP [9] and modified-OMP [10], have been considered in such applications. Moreover, basis pursuit (BP) algorithms have also been shown to exhibit robustness as compared to other CS techniques and also better estimation performance than the MP-based solutions, at the expense of increased computational complexity [11].

Nonetheless, it was pointed out in several studies that combining the aforementioned algorithms with other algorithms can boost the behavior of the communication system. This enhancement can be seen as a reduction in the average mean square error (MSE) of the estimated channel parameters, and consequently, a lower symbol error rate (SER). In our previous works [12], [13], we considered Rician fading for UWAC systems that operate in shallow water. The algorithm developed in [12] combines an MP algorithm with a maximum *a posteriori* probability (MAP) algorithm for colored noise. Moreover, this algorithm was extended to OMP-MAP in [13], and evaluated for different fading models as well as for impulsive noise and was shown to be robust compared with the FISTA algorithm [11], which is a member of the BP family. Finally, the work presented in [14] considers

Manuscript received December 3, 2020; revised January 22, 2021; accepted January 24, 2021. Date of publication February 1, 2021; date of current version March 10, 2021. This work was supported in part by the Turkish Scientific and Research Council (TUBITAK) under Grant 1140029 and in part by the U.S. National Science Foundation under Grant CCF-1908308. The review of this article was coordinated by Prof. K. Le. (*Corresponding author: Mhd Tahssin Altabbaa*.)

Erdal Panayirci is with the Department of Electrical and Electronics Engineering, Kadir Has University, Istanbul 34083, Turkey (e-mail: eepanay@khas.edu.tr).

Mhd Tahssin Altabbaa is with the Department of Electrical and Electronics Engineering, Istanbul Yeni Yüzyıl University, Istanbul 34010, Turkey (e-mail: tahsin@ieec.org).

H. Vincent Poor is with the Department of Electrical Engineering, Princeton University, Princeton, NJ 08544 USA (e-mail: poor@princeton.edu).

Digital Object Identifier 10.1109/TVT.2021.3056004

combining the MP algorithm with the expectation-maximization (EM) approach for relay-based UWAC systems.

Furthermore, wireless communication with antenna diversity has also been introduced to UWACs. Hence, diversity enables the receiver to overcome the fast-fading channel characteristics of the underwater environment. The works in [15], [16] utilize Alamouti space-time block coding (STBC), assuming OFDM transmission. The proposed approach in [15] first combines EM and MAP algorithms on each OFDM subcarrier in the frequency domain with the Karhunen-Loève expansion for complexity reduction. Then, the ESPRIT (Estimation of Signal Parameters via Rotational Invariant Technique) algorithm [17] was proposed to exploit the underwater channel sparsity, which leads to finer channel estimation. The authors of [16] investigated Alamouti STBC with OFDM for high-rate UWACs over time-varying channels where the diversity gain was exploited by the adaptive multi-channel receiver.

On the other hand, several contributions have considered space-frequency block coded (SFBC) techniques in UWACs. SFBC-based UWAC systems have an advantage over the STBC-based ones in that the adjacent subcarriers of the multicarrier communication system can be assumed approximately constant [18]. Consequently, contributions, such as [18] and [19], propose an adaptive channel estimation method for reducing pilot overhead and allowing simple data detection.

More interestingly, the authors of [20] have proposed an interesting delay estimation algorithm based on *Doppler focusing*. The algorithm was developed for target detection in radar systems for the case of targets having very close delay values. The algorithm focuses on a specific Doppler frequency, combining the received signals coming from different targets with appropriate Doppler frequencies coming together in phase. Then the problem is reduced to a one-dimensional CS problem and appropriate time delays are recovered with much lower computational complexity.

In this paper, we assume sparse underwater acoustic channels that undergo Rayleigh fading coupled with Alamouti's SFBC scheme with two transmitting and multiple receiving antennas. The proposed *non-data aided* channel estimation algorithm first estimates the underwater channel transfer function in the frequency domain considering the MAP criterion using the EM algorithm. Thus, the sparse channel impulse response that best matches the estimated channel transfer function is found by estimating the path delays and Doppler scaling factors by the proposed delay focusing algorithm. Then, time-varying complex-valued channel path gains are estimated using least squares (LS), making use of a basis expansion model (BEM) based on the orthonormal discrete Legendre polynomials (DLP). DLP-BEM has the advantage of being independent of the channel statistics, and hence, the expansion coefficients become uncorrelated as the OFDM frame length increases.

The main contributions of the paper are as follows:

- A computationally efficient non-data aided MAP channel estimation algorithm is proposed, estimating the channel frequency response of the $2 \times n_R$ UWA MIMO channels in Alamouti SFBC OFDM systems. It is shown by computer simulations that this algorithm achieves much better MSE performance with fewer pilot symbols than the conventional pilot-aided channel estimation techniques.

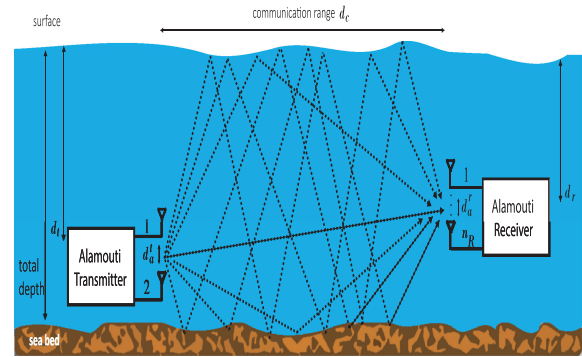


Fig. 1. Alamouti-based OFDM-UWA communications system diagram.

- This work assumes that each underwater channel path experiences different Doppler scale factors. Whereas the work in [8] assumes that all channel paths experience the same Doppler scale factor and the channel gains are constant. Consequently, as a result of the fine Doppler compensation, no Doppler “spread” is assumed to be present in the received signal anymore, the signal is assumed to have an uncompensated residual Doppler “shift”.
- A new algorithm for sparse channel estimation is presented for the channel path delays and Doppler scales estimation based on delay focusing, which is a modified version of the Doppler focusing algorithm introduced by [20] that reduces the computational complexity of the channel delay and Doppler spread estimations in a great deal.
- The sparse channel impulse responses formed by the estimated channel path gains and delays enable a robust solution that best matches the estimated channel transfer functions. Consequently, the computer simulations show that the new and refined channel estimation transfer function computed by means of those impulse responses improves the MSE and SER performances substantially.

The remainder of this paper is organized as follows. In, Section II, the transmit diversity according to Alamouti's scheme for a space-frequency coded OFDM system is presented. The discrete UWAC sparse channel model is presented in Section III. Section IV presents the MAP-EM channel estimation algorithm and Section V includes the final refined sparse channel impulse response estimation. Section VI includes the equalization and data detection operations. Section VII presents the complexity of the proposed approach and the computer simulation results with their corresponding underwater acoustic channel generation. Finally, conclusions are given in Section VIII.

II. TRANSMIT DIVERSITY SCHEME FOR ALAMOUTI SFBC-OFDM SYSTEMS

In this paper, a generalized model of Alamouti's [21] space-frequency block coded (SFBC) transmit diversity technique is applied for an OFDM-based underwater acoustic communication (UWAC) system, as shown in Fig. 1. Consequently, by introducing two-transmit antennas and n_R receiving antennas, a $2n_R$ diversity can be achieved. OFDM is used with K equally spaced subcarriers at $\Delta f = B/K$ within the system bandwidth B Hz. With the OFDM symbol duration $T = 1/\Delta f$, consequently, a cyclic prefix $T_{CP} \geq \tau_{\max}$, τ_{\max} , being the maximum multipath

spread of the UWA channel, is added to the complete OFDM symbol with duration of $T_{\text{OFDM}} = T + T_{CP}$. The OFDM subcarriers are first divided into groups of even (“*e*”) and odd (“*o*”) subcarriers ($2k$) and $(2k + 1)$, where $k = 0, 1, \dots, K/2 - 1$. Let the data vector transmitted during the OFDM block instant n , within a frame consisting of M OFDM symbols, as $\mathbf{d}(n) = [d_0(n), d_1(n), \dots, d_{K-1}(n)]^T$, where $d_k(n)$ is the k th component of the serial data symbol to be transmitted, during the block instant n , on the k th subcarrier. Based on the subchannel grouping, $\mathbf{d}(n)$ can be decomposed into two data vectors $\mathbf{d}_e(n)$ and $\mathbf{d}_o(n)$, whose components correspond to the even and odd components as follows.

$$\begin{aligned} \mathbf{d}_e(n) &= [d_0(n), d_2(n), \dots, d_{K-4}(n), d_{K-2}(n)]^T, \\ \mathbf{d}_o(n) &= [d_1(n), d_3(n), \dots, d_{K-3}(n), d_{K-1}(n)]^T. \end{aligned} \quad (1)$$

Based on the Alamouti encoding, $\mathbf{d}_e(n)$ and $\mathbf{d}_o(n)$ are transmitted from the two antennas at a given signaling interval and during the next signaling interval. Consequently, $-\mathbf{d}_e^*(n)$ and $\mathbf{d}_o^*(n)$ are transmitted from the first and the second transducers, respectively, where $(*)$ stands for the complex conjugation.

The received signal sequence, obtained from the r th ($r = 1, 2, \dots, n_R$) receiving antenna, can also be parsed in an even and odd blocks of K subcarriers as $\mathbf{Y}_e^r(n) = [Y_0^r(n), Y_2^r(n), \dots, Y_{K-2}^r(n)]^T$ and $\mathbf{Y}_o^r(n) = [Y_1^r(n), Y_3^r(n), \dots, Y_{K-1}^r(n)]^T$. The received signal can then be expressed as

$$\mathbf{Y}_e^r(n) = \mathcal{D}_e(n)\mathbf{H}_e^{1,r}(n) + \mathcal{D}_o(n)\mathbf{H}_e^{2,r}(n) + \mathbf{V}_e^r(n), \quad (2)$$

$$\mathbf{Y}_o^r(n) = -\mathcal{D}_o^\dagger(n)\mathbf{H}_o^{1,r}(n) + \mathcal{D}_e^\dagger(n)\mathbf{H}_o^{2,r}(n) + \mathbf{V}_o^r(n), \quad (3)$$

where the $K/2 \times K/2$ diagonal matrices $\mathcal{D}_e(n)$ and $\mathcal{D}_o(n)$ hold the $\mathbf{d}_e(n)$ and $\mathbf{d}_o(n)$ elements, respectively, and \dagger denotes the conjugate transpose. For $t = 1, 2$, and $r = 1, 2, \dots, n_R$, $\mathbf{H}_e^{t,r}(n) = [H_0^{t,r}(n), H_2^{t,r}(n), \dots, H_{K-2}^{t,r}(n)]^T \in K/2$ and $\mathbf{H}_o^{t,r}(n) = [H_1^{t,r}(n), H_3^{t,r}(n), \dots, H_{K-1}^{t,r}(n)]^T \in K/2$, denote the even and odd elements of the UWA frequency-domain channel transfer functions between the t^{th} transmit and the r^{th} receive antennas. Finally, $\mathbf{V}_e^r(n)$ and $\mathbf{V}_o^r(n)$ represent $K/2$ -dimensional vectors of the zero mean and independent identically distributed Gaussian additive noise with a variance of $\sigma^2/2$ per dimension.

From equations (2) and (3), it can be seen that the transducers transmit the information symbols $\mathcal{D}_e(n)$ and $\mathcal{D}_o(n)$ over two consecutive adjacent subchannel groups over two different channels. For each n , the Alamouti assumption is then used for the channel estimation and equalization and data detection.

Based on the work [18], we also assume that the channel variations to be negligible between two consecutive subcarriers in the space-frequency coding technique. That is, $\mathbf{H}_e^{1,r}(n) \approx \mathbf{H}_e^{1,r}(n)$ and $\mathbf{H}_e^{2,r}(n) \approx \mathbf{H}_e^{2,r}(n)$. Accordingly, this assumption allows omitting the dependence of $\mathbf{H}_e^{1,r}(n)$ and $\mathbf{H}_e^{2,r}(n)$ on the odd channel components [19]. Consequently, dropping subscripts “*e*” and “*o*,” equations (2) and (3) can be expressed in a matrix as

$$\begin{bmatrix} \mathbf{Y}_e^r(n) \\ \mathbf{Y}_o^r(n) \end{bmatrix} = \begin{bmatrix} \mathcal{D}_e(n)\mathcal{D}_o(n) \\ -\mathcal{D}_o^\dagger(n)\mathcal{D}_e^\dagger(n) \end{bmatrix} \begin{bmatrix} \mathbf{H}^{1,r}(n) \\ \mathbf{H}^{2,r}(n) \end{bmatrix} + \begin{bmatrix} \mathbf{V}_e^r(n) \\ \mathbf{V}_o^r(n) \end{bmatrix}. \quad (4)$$

Equation (4) can be represented as

$$\mathbf{Y}^r(n) = \mathcal{D}(n)\mathbf{H}^r(n) + \mathbf{V}^r(n). \quad (5)$$

Based on (5), the main objective of our work is to develop, first, a non-data aided-based channel estimation algorithm according to the MAP criterion. The estimated channel, $\hat{\mathbf{H}}^r(n) = [\hat{\mathbf{H}}^{1,r}(n), \hat{\mathbf{H}}^{2,r}(n)]^T$, is an observed frame of M OFDM symbols for $n = 0, 1, \dots, M - 1$. Then, exploiting the sparse nature of the UWA channels, sparse channel impulse responses, $\hat{\mathbf{h}}^r(n) = [\hat{\mathbf{h}}_1^{1,r}(n), \hat{\mathbf{h}}_1^{2,r}(n)]^T$, are found that best matches the channel model for the given estimates $\{\hat{\mathbf{H}}^{t,r}(n)\}_{n=0}^{M-1}$ and a desired degree of sparseness, L , as inputs. Finally, detection will be performed on equalized data based the least square (LS) estimation algorithm.

III. DISCRETE UWA CHANNEL REPRESENTATION

The UWA channel is time varying and its impulse response (CIR) is sparse. Between t ($t = 1, 2$)th transmitting antenna and r ($r = 1, 2, \dots, n_R$)th receiving antenna, the CIR can be characterized, during n th OFDM block (interval $\tau \in (nT, (n+1)T)$), by

$$c^{t,r}(n, \tau) = \sum_{\ell=0}^{L-1} A_\ell^{t,r}(n) \delta(\tau - \tau_\ell^{t,r}(n)), \quad (6)$$

where, $A_\ell^{t,r}(n)$, L and $\tau_\ell^{t,r}(n)$ respectively denote the real channel path amplitudes, the number of paths with significant powers and the time-varying path delays. For a duration of one OFDM symbol, the path amplitudes are assumed to be slowly time varying with the block index n . In UWA communications, path delays, $\tau_\ell^{t,r}(n)$, caused by the motion of the transceiver pair, the ray reflections as a result of the sound speed variations, or the scattering of the moving sea surface [22]. In addition, the frequency-dependent channel Doppler effects is mitigated by resampling operation carried out on the received passband signal with an estimated resampling factor. This factor corresponds to a rough Doppler estimate and reflects the relative deletion/compression experienced by the received signal. Then, a fine Doppler shift compensation is carried out on the received baseband signal. Hence, we assume *a priori* that the receiver has the ability to estimate and compensate the Doppler shift perfectly, then the time variations of the path delays can be well approximated by

$$\tau_\ell^{t,r}(n) = \tau_\ell^{t,r} - b_\ell^{t,r} n T_{\text{OFDM}}, n = 0, 1, \dots, M - 1, \quad (7)$$

where $b_\ell^{t,r}$'s are the path dependent Doppler rates, which are spread around zero between $[-b_{\text{max}}, +b_{\text{max}}]$ [8]. Note that, $b_{\text{max}} = v_{\text{max}}/c$, with maximum velocity v_{max} m/s and the sound speed $c = 1500$ ms, typically does not exceed 10^{-4} [8]. Following the work [19], we assume that $b_\ell^{t,r} \approx b_\ell^t$, which corresponds to the case in which both transmitting and receiving units are co-located and the major cause of the motion is the motion of the transmitter.

The model in (6) represents only the real-valued sparse channel path gains $A_\ell^{t,r}$ obtained experimentally or by a ray-tracing technique. However, there are many diffuse intrapath gains $A_{\ell,i}^{t,r}$ and intrapath delays $\delta\tau_{\ell,i}^{t,r}$ that characterize the random movements of the scattering points [23]. Consequently, the overall discrete transfer function of the complex-equivalent baseband

time-varying multipath UWA channels between each transmit antenna to the receive antennas can be expressed from (6) as

$$H_k^{t,r}(n) = \sum_{\ell=0}^{L-1} h_{\ell}^{t,r}(n) \exp\left(-j \frac{2\pi k \tilde{\tau}_{\ell}^{t,r}(n)}{K}\right), \quad (8)$$

where $k = 0, 1, \dots, K-1; n = 0, 1, \dots, M-1$, $\tilde{\tau}_{\ell}^{t,r}(n) = \tau_{\ell}^{t,r}(n)/T_s$ is the ℓ^{th} normalized path delays and $T_s = T/K$ being the sampling interval and the small-scale fading coefficients in (8) are defined as [23]

$$h_{\ell}^{t,r}(n) = \sum_i A_{\ell,i}^{t,r}(n) \exp\left(-j2\pi f_c \delta \tilde{\tau}_{\ell,i}^{t,r}(n)\right). \quad (9)$$

Hence, assuming the components in the summation above are independent and identically distributed (i.i.d.), by the central limit theorem, the channel coefficients, $h_{\ell}^{t,r}(n)$, in (9) are close to complex Gaussian random variables with power delay profile $P_D(\tilde{\tau}_{\ell}^{t,r}(n))$, for each OFDM block index n . According to [24], the power delay profile of UWA channels can quite fit into the exponential decay model expressed as $P_D(\tilde{\tau}_{\ell}^{t,r}(n)) = C \exp(-\tilde{\tau}_{\ell}^{t,r}(n)/\tau_{\text{rms}})$ where C is a normalizing constant, chosen to satisfy $C \sum_{\ell=0}^{L-1} \exp(-\tilde{\tau}_{\ell}^{t,r}(n)/\tau_{\text{rms}}) = 1$. However, each channel path gain, $|h_{\ell}^{t,r}(n)|$, can be assumed to follow a different distribution. This is due to the moving conditions that characterize the UWACs. For UWAC systems that operate in a long distance communication range, large sea dynamics prevent the receiver from acquiring the line-of-sight path. Hence, channel path gains are assumed to follow the Rayleigh distribution, which is considered in this work. Furthermore, to find a statistically equivalent model for (9), to generate the UWA channels in the time domain for our computer simulations, the correlation function and the power spectral density of $h_{\ell}^{t,r}(n)$ are derived whose details are given in Appendix-A.

On the other hand, based on the Alamouti assumption adopted in our paper, expressed for space-frequency coding, the frequency response of the UWA channel should not change much over two consecutive carries $H_{2k}^{t,r}(n) \approx H_{2k+1}^{t,r}(n)$. This can be shown as follows. Given the delays in (7), the channel transfer function (8) can be decomposed as

$$H_k^{t,r}(n) = \tilde{H}_k^{t,r}(n) e^{-j\theta_k^t(n)}$$

where

$$\tilde{H}_k^{t,r}(n) \triangleq \sum_{\ell=0}^{L-1} h_{\ell}^{t,r}(n) e^{-j \frac{2\pi k \tau_{\ell}^{t,r}}{T_s K}},$$

and $\theta_k^t(n) \triangleq \frac{2\pi k b^t n T_{\text{OFDM}}}{T_s K}$. Hence, as far as the Alamouti assumption is concerned, it will hold if

$$\tilde{H}_{k+1}^{t,r}(n) \approx \tilde{H}_k^{t,r}(n) \text{ and } \exp\left(-j \frac{2\pi b_{\ell}^t n T_{\text{OFDM}}}{T_s K}\right)$$

$$\approx 0 \text{ for all } k, t, r.$$

The first condition hold if the OFDM system is properly designed in such a way that initial synchronization is sufficiently accurate with respect to each transmitter. That is, neither channel channel exhibit significant phase rotation across the carriers. This is a reasonable assumption for collocated transmitters. The second condition above will also hold since $T_{\text{OFDM}}/KT_s \approx 1$ and the residual Doppler spread factors b_{ℓ}^t typically do not exceed 10^{-4} at the output of the resampling process [19].

Finally, normalized to unity, the time-varying discrete frequency-domain channel autocorrelation coefficients at each time index, $n = 1, 2, \dots, M$, defined as $\tau_n(u) = \{H_k^{t,r}(n)H_{k+u}^{t,r*}(n)\}$ and can be expressed as

$$\tau_n(u) = \text{sinc}\left(\frac{2N_{\text{OFDM}}b_{\text{max}}nu}{K}\right) \times \frac{1 - \exp(-L_{\text{CP}}(1/\tau_{\text{rms}} + j2\pi m/K))}{\tau_{\text{rms}}(1 - e^{-L_{\text{CP}}/\tau_{\text{rms}}})(1/\tau_{\text{rms}} + j2\pi m/K)}, \quad (10)$$

for $k, u = 0, 2, \dots, K/2 - 1$. $N_{\text{OFDM}} = T_{\text{OFDM}}/T_s$, $L_{\text{CP}} = T_{\text{CP}}/T_s$ and $\text{sinc}(x) = \sin(\pi x)/\pi x$. Derivations of this expression are given in Appendix-B.

IV. MAP-EM CHANNEL ESTIMATION

In this section, the non-data-aided channel estimation algorithm is presented. Based on orthogonal representation of the discrete multipath sparse channel, the algorithm utilizes the maximum *a posterior* probability and the Expectation Maximization techniques (MAP-EM). In this technique, only a few pilot symbols are used for the initialization of the EM algorithm. Assuming all the channels between the t^{th} transmit antennas for $t = 1, 2$ and the r^{th} receive antennas for $r = 1, 2, \dots, n_R$ have the same effective delays values (τ_{rms}) and same maximum Doppler spread (b_{max}), the channel correlation matrix is independent of the transmit and receive antenna indexes, (t, r) . For notational simplicity, we ignore the parameter n in the subsequent formulations and use the notations $\mathbf{H}^{t,r}$, \mathbf{Y}^r , $\mathbf{G}^{t,r}$, \mathcal{D} and $\tau(u)$ instead of $\mathbf{H}^{t,r}(n)$, $\mathbf{Y}^r(n)$, $\mathbf{G}^{t,r}(n)$, $\mathcal{D}(n)$ and $\tau_n(u)$, respectively, throughout this section. Utilizing the singular value decomposition (SVD), the frequency-domain channel autocorrelation matrix ($K/2 \times K/2$), $\mathfrak{R}[k, k+u] = \tau(u)$, can be defined as $\mathfrak{R} = \mathbf{U}\mathbf{\Lambda}\mathbf{U}^{\dagger}$, where $\mathbf{\Lambda}$ is a $K/2 \times K/2$ diagonal matrix with elements $\lambda_0 > \lambda_1 > \dots > \lambda_{K/2-1}$ representing the eigenvalues and $\mathbf{U} = [\mathbf{u}_0, \mathbf{u}_1, \dots, \mathbf{u}_{K/2-1}]$, where $\mathbf{u}_i \in \mathcal{C}^{K/2}$ are the eigenvectors of \mathfrak{R} . By applying the linear transformation, $\mathbf{H}^{t,r} = \mathbf{U}\mathbf{G}^{t,r}$, all components of $\mathbf{G}^{t,r} \in \mathcal{C}^{K/2}$ become independent with zero-mean Gaussian random variables and variances $\{\lambda_i\}_{i=0}^{K/2-1}$. Defining $\tilde{\mathbf{\Lambda}} = \text{diag}(\mathbf{\Lambda}, \mathbf{\Lambda})$, the prior probability density function (pdf) of $\mathbf{G}^r = [(\mathbf{G}^{1,r})^T, (\mathbf{G}^{2,r})^T]^T$ can then be expressed as

$$p(\mathbf{G}^r) \sim \exp(-\mathbf{G}^{r\dagger} \tilde{\mathbf{\Lambda}}^{-1} \mathbf{G}^r). \quad (11)$$

Conditional pdf of the received signal, \mathbf{Y}^r , given the transmitted data symbols \mathcal{D} coded according to Alamouti's scheme, and the discrete channel representation, $\mathbf{G}^{t,r}$, as well as taking into account the independence of the noise components, can be expressed as

$$p(\mathbf{Y}^r | \mathcal{D}, \mathbf{G}^r) \sim \exp\left\{-\frac{1}{\sigma^2} (\mathbf{Y}^r - \mathcal{D}\tilde{\mathbf{U}}\mathbf{G}^r)^{\dagger} (\mathbf{Y}^r - \mathcal{D}\tilde{\mathbf{U}}\mathbf{G}^r)\right\}, \quad (12)$$

where $\tilde{\mathbf{U}} = \text{diag}[\mathbf{U}, \mathbf{U}] \in \mathcal{C}^{K \times K}$.

In the proposed non-data-aided MAP channel estimation algorithm, $\hat{\mathbf{G}}_{\text{MAP}}^r$ is chosen to maximize the posterior pdf as,

$$\hat{\mathbf{G}}_{\text{MAP}}^r = \arg \max_{\mathbf{G}^r} p(\mathbf{G}^r | \mathbf{Y}^r). \quad (13)$$

It is mathematically intractable to find a direct solution of (13). In order to overcome this dilemma, the iterative nature of the EM algorithm can simplify it and re-estimate the \mathbf{G}^r , in a mathematically feasible way, such that, a monotonic increase in the *a posteriori* conditional pdf in (13) can be guaranteed. This monotonic increase can be realized utilizing the maximization of the following auxiliary function

$$Q(\mathbf{G}^r | \mathbf{G}^{r(q)}) = \sum_{\mathcal{D}} p(\mathbf{Y}^r, \mathcal{D}, \mathbf{G}^{r(q)}) \log p(\mathbf{Y}^r, \mathcal{D}, \mathbf{G}^r), \quad (14)$$

where the summation is taken over all possible transmitted data coded signals and $\mathbf{G}^{r(q)}$ is the estimation of \mathbf{G}^r at the q^{th} iteration. Note that, $p(\mathbf{Y}^r, \mathcal{D}, \mathbf{G}^r) \sim p(\mathbf{Y}^r | \mathcal{D}, \mathbf{G}^r) p(\mathcal{D} | \mathbf{G}^r)$, since the data symbols, $\mathcal{D} = \{d_{2k}(n), d_{2k+1}(n)\}$, are assumed to be transmitted independently of each other and identically distributed and by the fact that \mathcal{D} is independent of \mathbf{G}^r . Hence, (14) can be evaluated by means of the expressions (11) and (12). Given the received signal, \mathbf{Y}^r , the EM algorithm starts with an initial value $\mathbf{G}^{r,(0)}$ of the unknown channel parameters \mathbf{G}^r . The $(q+1)^{\text{th}}$ estimate of \mathbf{G}^r is obtained by the maximization step and described by

$$\mathbf{G}^{r(q+1)} = \arg \max_{\mathbf{G}^r} Q(\mathbf{G}^r | \mathbf{G}^{r(q)}), \quad (15)$$

where $\mathbf{G}^{r(q+1)} = [(\mathbf{G}^{1,r(q+1)})^T, (\mathbf{G}^{2,r(q+1)})^T]^T$. As described in Appendix-C, $\mathbf{G}^{t,r(q+1)}$ for $t = 1, 2$ can be obtained as

$$\begin{aligned} \mathbf{G}^{1,r(q+1)} &= \Xi^{-1} \mathbf{U}^\dagger \left(\Gamma_{1,r}^{(q)\dagger} \mathbf{Y}_e^r - \Gamma_{2,r}^{(q)} \mathbf{Y}_o^r \right), \\ \mathbf{G}^{2,r(q+1)} &= \Xi^{-1} \mathbf{U}^\dagger \left(\Gamma_{2,r}^{(q)\dagger} \mathbf{Y}_e^r + \Gamma_{1,r}^{(q)} \mathbf{Y}_o^r \right), \end{aligned} \quad (16)$$

where $\Xi \triangleq \mathbf{U}^\dagger (\Upsilon_{1,r}^{(q)} + \Upsilon_{2,r}^{(q)}) \mathbf{U} + \sigma^2 \mathbf{\Lambda}^{-1}$. $\Gamma_{t,r}^{(q)}$ and $\Upsilon_{t,r}^{(q)}$ are diagonal matrices of size $(K/2 \times K/2)$ that represent the *a posteriori* probabilities and the average power of the data symbols, respectively, at the q^{th} iteration step. Exact expressions for their k^{th} diagonal components, $\Gamma_{t,r}^{(q)}(k)$ and $\Upsilon_{t,r}^{(q)}(k)$ are derived in Appendix-D for the square M -QAM signal constellation. For QPSK signaling, by substituting $M = 4$ in Eq. (D.1), we obtain the result given by [26] as

$$\begin{aligned} \Gamma_{t,r}^{(q)}(k) &= \frac{1}{\sqrt{2}} \tanh \left(\frac{\sqrt{2}}{\sigma^2} \Re \{ Z_{t,r}^{(q)}(k) \} \right) \\ &\quad + \frac{j}{\sqrt{2}} \tanh \left(\frac{\sqrt{2}}{\sigma^2} \Im \{ Z_{t,r}^{(q)}(k) \} \right), \end{aligned} \quad (17)$$

$$\Upsilon_{t,r}^{(q)}(k) = 1. \quad (18)$$

where $\Re\{\cdot\}$ and $\Im\{\cdot\}$ denote the real and imaginary parts of a complex number, and exact expressions of $Z_{t,r}^{(q)}(k)$ for $t = 1, 2$ are derived in Appendix-D.

Consequently, by the convergence of the EM algorithm, the MAP estimate of $\mathbf{H}^{t,r}$ can then be obtained as

$$\hat{\mathbf{H}}_{MAP}^{t,r} = \mathbf{U} \hat{\mathbf{G}}_{MAP}^{t,r}, \text{ for } t = 1, 2; r = 1, 2, \dots, n_R, \quad (19)$$

where, $\hat{\mathbf{G}}_{MAP}^{t,r}$ is the EM-converged value of $\mathbf{G}^{t,r(q)}$ in (16) after some number of iterations.

A. Initialization

The initial values of the unknown channel parameters, $\mathbf{G}^{t,r(0)}$, are chosen by means of $2P$ pilot symbols $\{d_{2i_p}(n)\}$ and $\{d_{2i_p+1}(n)\} \in \mathcal{A}_p$ modulated by the $2i_p^{\text{th}}$ and $(2i_p + 1)^{\text{th}}$ subcarriers, transmitted at time slot $\{n\}$ for $p = 1, 2, \dots, P$, $i_p \in \{0, 1, \dots, K-1\}$. The received signal in (5), at the pilot subcarriers, $i_p \in \mathcal{P} = \{i_1, i_2, \dots, i_P\}$, of the two successive OFDM symbols can be expressed as

$$\mathbf{Y}_p^r = \mathcal{D}_p \mathbf{H}_p^{t,r} + \mathbf{V}_p^r, \quad (20)$$

where $\mathbf{Y}_p^r, \mathbf{H}_p^{t,r}, \mathbf{V}_p^r \in \mathbb{C}^{2P}$ and $\mathcal{D}_p \in \mathbb{C}^{2P \times 2P}$ are obtained from $\mathbf{Y}^r, \mathbf{H}^{t,r}, \mathbf{V}^r \in \mathbb{C}^K$, and $\mathcal{D} \in \mathbb{C}^{K \times K}$. Consequently, applying the least squares (LS) estimation, the channel can then be obtained from (4) as

$$\begin{aligned} \hat{\mathbf{H}}_p^{1,r}(n) &= \Delta^{-1} (\mathcal{D}_{p,e}^\dagger(n) \mathbf{Y}_{p,e}^r(n) - \mathcal{D}_{p,o}(n) \mathbf{Y}_{p,o}^r(n)) \in \mathbb{C}^P, \\ \hat{\mathbf{H}}_p^{2,r}(n) &= \Delta^{-1} (\mathcal{D}_{p,o}^\dagger(n) \mathbf{Y}_{p,e}^r(n) + \mathcal{D}_{p,e}(n) \mathbf{Y}_{p,o}^r(n)) \in \mathbb{C}^P, \end{aligned} \quad (21)$$

where $\Delta = \|\mathcal{D}_{p,o}(n)\|_F^2 + \|\mathcal{D}_{p,e}(n)\|_F^2$ and “ F ” denotes the Frobenius norm. Note that for constant envelope signaling schemes with unit average power, $\Delta = \frac{1}{2} \mathbf{I}_{K/2}$. Consequently, the initial channel parameters are selected as $\hat{\mathbf{G}}_p^{t,r(0)}(n) = \mathbf{U} \hat{\mathbf{H}}_p^{t,r}(n)$.

V. FINAL REFINED SPARSE CHANNEL ESTIMATION

Channel frequency response estimates, $\hat{\mathbf{H}}^{t,r}(n)$, obtained in the previous section do not take the sparse characteristic of the channel into account. However, UWA channels are usually sparse in nature, whose sparse channel impulse response is characterized by the number of paths, the path gains, the Doppler spread, and the path delays. If these parameters could be estimated, then, a sparse solution of the UWA channel impulse response, $\mathbf{h}^{t,r}(n)$, can be found. Define $\mathbb{F}_L \in K/2 \times L$ as the discrete Fourier transform (DFT) matrix, hence this sparse solution that best matches the model $\hat{\mathbf{H}}_{MAP}^{t,r}(n) = \mathbb{F}_L \mathbf{h}^{t,r}(n)$ for the estimated values $\hat{\mathbf{H}}_{MAP}^{t,r}(n)$ and fully guarantees an estimated UWA sparse channel. This would lead to significantly improved channel estimation performance as well as the computational complexity of the resulting estimation algorithm. The compressed sensing (CS) have been shown to be very effective for one-shot sparse channel estimation [22]. However, in UWACs, the sparsity does not always hold. Consequently, this may not reflect a truly sparse channel response due to the fact that the normalized path delays are non-integer in the equivalent discrete-time baseband representation, which affects the estimation and deteriorates the final estimated channel coefficient. One way to solve this problem in the CS approach is to use a so-called, *dictionary matrix* with finer delay resolution. However, the size of the dictionary grows as the resolution increases. Also, as the number of different parameters to be estimated increases more than one, like estimating the path delays, the paths gains and the Doppler scaling factors, computational complexity of directly applying a CS method such as orthogonal matching pursuit (OMP) [9] would be substantially higher and make those algorithms difficult to apply in dynamic environments such as UWA channels. In the following subsection we propose a computationally efficient technique, based on a novel approach

called *Delay Focusing* that alleviates these difficulties encountered.

A. Estimation of Path Delays and Doppler Scaling Factors by Delay Focusing

Inspiring by the idea of Doppler focusing presented in [20], we now develop a novel signal processing algorithm, to estimate the channel path delays $\tau_\ell^{t,r}(n)$ and the Doppler spreading factors $b_\ell^t(n)$, iteratively, in a given OFDM frame consisting of M OFDM symbols, for $n = 0, 1, \dots, M-1$.

Let the one-shot channel estimates of the channel transfer functions, $\hat{\mathbf{H}}^{t,r}(0), \hat{\mathbf{H}}^{t,r}(1), \dots, \hat{\mathbf{H}}^{t,r}(M-1)$, are obtained by the technique presented in Sec. IV, where $\hat{\mathbf{H}}^{t,r}(n) \equiv \mathbf{H}_{MAP}^{t,r}(n)$. For notational simplicity, we omit (t, r) in the following derivations. The k^{th} component of $\hat{\mathbf{H}}^{t,r}(n)$ is obtained from (8) as

$$\begin{aligned} \hat{H}_k(n) &= \sum_{\ell=0}^{L-1} h_\ell(n) \exp\left(-j \frac{2\pi k \tilde{\tau}_\ell(n)}{K}\right), k = 0, 1, \dots, K-1. \end{aligned} \quad (22)$$

The complex-valued random path gains, $h_\ell(n)$, and the normalized path delays are modeled as in (9) and (7), respectively. Substituting (7) in (22), it follows that

$$\hat{H}_k(n) = \sum_{\ell=0}^{L-1} h_\ell(n) e^{-j2\pi k \tilde{\tau}_\ell / K} e^{j2\pi k n b_\ell N_{\text{OFDM}} / K}. \quad (23)$$

We now perform the operation, called the *delay focusing*, for a specific normalized path delay, $\tilde{\tau}$, defined as [20]:

$$\begin{aligned} \Psi_{\tilde{\tau}}(n) &\triangleq \sum_{k=0}^{K-1} \hat{H}_k(n) e^{j2\pi k \tilde{\tau} / K} \\ &= \sum_{\ell=0}^{L-1} h_\ell(n) \sum_{k=0}^{K-1} e^{j2\pi k (\tilde{\tau} - \tilde{\tau}_\ell) / K} e^{j2\pi k n b_\ell N_{\text{OFDM}} / K}. \end{aligned} \quad (24)$$

In (24), for a given $\tilde{\tau}$, channel path delay, $\tilde{\tau}_\ell$, within a time interval of width 1 around $\tilde{\tau}$ called *focus zone*. Hence, the exponential terms will be approximately zero for $|\tilde{\tau} - \tilde{\tau}_\ell| > 1/2$. Also since the path gains, $h_\ell(n)$, are slowly time varying, it can be approximated by its average over a frame of M OFDM symbols as

$$h_\ell(n) \approx \bar{h}_\ell = \frac{1}{M} \sum_{n=0}^{M-1} h_\ell(n). \quad (25)$$

Hence, paths with delays $\tilde{\tau}_\ell$ *not in focus* will be canceled out, yielding the equation (24) to be approximately expressed by,

$$\Psi_{\tilde{\tau}}(n) \approx K \bar{h}_\ell \text{sinc}(N_{\text{OFDM}} n b_\ell) e^{-j\pi n (K-1) b_\ell N_{\text{OFDM}}}, \quad (26)$$

where $n = 0, 1, \dots, M-1; \ell = 0, 1, \dots, L-1$ for which $|\tilde{\tau} - \tilde{\tau}_\ell| \leq 1/2$. By this approach then, the sum of the exponents in (24) will achieve a SNR boost of approximately K in the focus zone. Note that by delay focusing, the joint estimation of Doppler scaling factors and the delays is reduced only to the Doppler estimation problem, with increased amplitude for improved performance against noise.

Algorithm 1: Joint Estimation of Delays and Doppler Scaling Factors by Discrete Delay Focusing.

Input: $\{\Psi_q(n)\}_{1 \leq q \leq N_\tau}^{0 \leq n \leq M-1}$, computed from (27); L (Number of paths); M (OFDM frame length); b_{max} (Maximum Doppler spread), τ_{max} (Maximum delay spread)
Output: Estimated path parameters $\{\hat{b}_\ell, \hat{\tau}_\ell\}_{\ell=0}^{L-1}$
for $i = 0$ to $L-1$ **do**
 $\{\hat{q}_\ell, \hat{b}_\ell\} \leftarrow \text{argmax}_{-b_{\text{max}} \leq b \leq b_{\text{max}} | 1 \leq q \leq N_\tau}$
 $\left| \sum_{n=0}^{M-1} \Psi_q(n) e^{j\pi n (K-1) N_{\text{OFDM}} b / K} \right|$
 $\hat{\tau}_\ell \leftarrow (\hat{q}_\ell - 1) \Delta\tilde{\tau}$
 $\hat{h}_\ell \leftarrow \frac{1}{MK} \sum_{n=0}^{M-1} \Psi_{\hat{q}_\ell}(n) e^{j\pi n (K-1) N_{\text{OFDM}} \hat{b}_\ell / K} \times$
 $(\text{sinc}(n N_{\text{OFDM}} \hat{b}_\ell))^{-1}$
for $q = 1$ to N_τ **do**
for $n = 0$ to $M-1$ **do**
 $\Psi_q(n) \leftarrow \Psi_q(n) - \hat{h}_\ell \sum_{k=0}^{K-1} e^{j2\pi k (\tilde{\tau}_q - \hat{\tau}_\ell) / K} \times$
 $e^{j2\pi k n \hat{b}_\ell N_{\text{OFDM}} / K}$
end for
end for
end for

The delay focusing operation in (24) is continuous on $\tilde{\tau}$ and can be applied to any $\tilde{\tau} \in [0, \tilde{\tau}_{\text{max}}]$. For each $\tilde{\tau}$, b_ℓ 's can be recovered from $\Psi_{\tilde{\tau}} = [\Psi_{\tilde{\tau}}(0), \dots, \Psi_{\tilde{\tau}}(M-1)]^T$ iteratively by jointly processing (24) for all values of $\tilde{\tau}$. This process, in each iteration, guarantees to recover one Doppler scaling value and removes its influence from $\Psi_{\tilde{\tau}}$. The iterative algorithm searches for largest b_ℓ first. After estimating each Doppler scaling, its influence is removed from the set of observations in order to reduce masking of weaker Doppler scalings.

For computational simplicity, the delay focusing, $\Psi_{\tilde{\tau}}$, can be implemented with $\tilde{\tau}$ discretized on a uniform grid of N_τ normalized path delays $\{\tilde{\tau}_q = (q-1)\Delta\tilde{\tau}\}_{q=1}^{N_\tau}$ at the discrete points $q = 1, 2, \dots, N_\tau$, as

$$\begin{aligned} \Psi_q(n) &= \sum_{k=0}^{K-1} \hat{H}_k(n) e^{j2\pi k \tilde{\tau}_q / K}, n = 0, 1, \dots, M-1. \end{aligned} \quad (27)$$

Then $\Psi_{\tilde{\tau}}(n)$ can be computed efficiently using a length K discrete Fourier transform (DFT) of a series $\hat{H}_k(n)$ for each $n = 1, 2, \dots, M-1$. Furthermore, since in UWA channels there is usually only one Doppler scaling factor associated with a path delay, delay focusing algorithm simplifies further. Algorithm 1 below describes this process in detail.

B. Estimation of Complex-Valued Path Gains

In a time-varying environment, the number of the path gains within one OFDM frame consisting of M OFDM symbols is ML . Exploiting the time correlation present in the channel, the number of parameters to be estimated can be reduced by using a basis expansion model (BEM) to model the time-variations of the channel path gains [27]. The ℓ th path gain within an OFDM frame, the channel coefficients, $h_\ell(n), n = 0, 1, \dots, M-1$, can be represented as weighted sums of M

orthogonal basis functions $\{\phi_q(n)\}$, $q = 0, 1, \dots, M - 1$ in the interval $[0, MN_{\text{OFDM}}T_s]$. However, for slowly varying channel path gains, $h_\ell(\cdot)$ can be seen as a lowpass operation that the effective Doppler frequency, B_d , can determine its bandwidth and it can be well approximated by the weighted sum of a substantially fewer number ($D \ll M$) of suitable orthonormal basis functions:

$$h_\ell(n) \approx \sum_{q=0}^{D-1} \phi_q(n) c_\ell(q), n = 0, 1, \dots, M - 1, \quad (28)$$

where $\mathbf{c}_\ell = [c_\ell(0), c_\ell(1), \dots, c_\ell(D - 1)]^T$ is the BEM coefficients vector. Once these coefficients are estimated, the channel gains, $h_\ell(n)$, can be computed and tracked from (28) with low complexity for $n = 0, 1, \dots, M - 1$ and $\ell = 0, 1, \dots, L - 1$ in a given OFDM frame. The dimension D of the basis expansion satisfies $D_{\text{lower}} \leq D \leq M$. The lower bound D_{lower} is given by $D_{\text{lower}} = \lceil 2B_{\text{max}}T_{\text{OFDM}}M + 1 \rceil$, where $\lceil \cdot \rceil$ is a ceiling operation and $B_{\text{max}} = \max_\ell \{B_\ell\}$. In our work, we utilize the basis expansion model (BEM), based on the orthonormal discrete Legendre polynomials (DLP), for representing the time variations of the UWA channel within an observation interval. According to [27], the DLP-BEM can be independent of the channel statistics and the associated expansion coefficients become uncorrelated as the number of observations M gets larger. Hence, DLP-BEM well suits the low-pass equivalent of the UWA channel using a small number of basis functions. The Legendre polynomials are generated using the Gram-Schmidt orthogonalization on the polynomials $\{1, n, n^2, \dots\}$ with respect to the time-varying UWA channel coefficients in a range of the middle point of the considered interval. They can be defined as $\phi_q(n) = \nu_q(n)/\xi_q$, where ξ_q denotes the normalization coefficient. The DLPs $\nu_q(n)$ and their corresponding normalization coefficients can be computed recursively as

$$\begin{aligned} \nu_q(n) &= \frac{(2q-1)(M-1-2n)}{q(M-q)} \nu_{q-1}(n) \\ &\quad - \frac{(q-1)(M+q-1)}{q(M-q)} \nu_{q-2}(n) \\ \xi_q &= \sqrt{\frac{(2q-1)(M+q)}{(2q+1)(M-q)}} \xi_{q-1}, \\ n &= 0, 1, \dots, M-1, q = 2, 3, \dots, D-1, \end{aligned} \quad (29)$$

with the following initial polynomials and coefficients

$$\begin{aligned} \nu_0(n) &= 1, \nu_1(n) = 1 - \frac{2n}{M-1}, \\ \xi_0 &= \sqrt{M}, \xi_1 = \sqrt{\frac{M(M+1)}{3(M-1)}}. \end{aligned} \quad (30)$$

Given the estimates $\hat{\mathbf{H}}(n)$ and $\hat{\tau}_\ell(n)$ for $n = 0, 1, \dots, M - 1$, obtained earlier, (23) can be expressed in vectorial form as

$$\hat{\mathbf{H}}(n) = \hat{\mathbf{F}}(n)\mathbf{h}(n) \quad (31)$$

where the (k, ℓ) th element of the matrix $\hat{\mathbf{F}}(\cdot) \in \mathbb{C}^{K \times L}$ is $\hat{\mathbf{F}}(n)[k, \ell] = \exp(-j\frac{2\pi\hat{\tau}_\ell(n)k}{K})$, $\mathbf{h}(n) = [h_0(n), h_1(n), \dots, h_{L-1}(n)]^T$. From (28), taking into account the fact that for $\ell = 0, 1, \dots, L - 1$, $h_\ell(n) = \phi^T(n)\mathbf{c}_\ell$, where

$\phi(n) = [\phi_0(n), \phi_1(n), \dots, \phi_{D-1}(n)]^T \in \mathcal{R}^D$, $\mathbf{h}(n)$ can be expressed in a matrix form as

$$\mathbf{h}(n) = \Phi(n)\mathbf{c} \quad (32)$$

where $\Phi(n) = \text{diag}\{\phi^T(n), \phi^T(n), \dots, \phi^T(n)\} \in \mathcal{R}^{L \times DL}$ and $\mathbf{c} = [\mathbf{c}_0, \mathbf{c}_1, \dots, \mathbf{c}_{L-1}]^L \in \mathbb{C}^{DL}$. Eq. (31) can then be written in a more compact form as

$$\hat{\mathbf{H}} = \text{diag}\{\hat{\mathbf{F}}(0), \hat{\mathbf{F}}(1), \dots, \hat{\mathbf{F}}(M-1)\} \mathbf{h} \quad (33)$$

where $\hat{\mathbf{H}} = [\hat{\mathbf{H}}^T(0), \hat{\mathbf{H}}^T(1), \dots, \hat{\mathbf{H}}^T(M-1)]^T \in \mathbb{C}^{MK}$, $\mathbf{h} = [\mathbf{h}^T(0), \mathbf{h}^T(1), \dots, \mathbf{h}^T(M-1)]^T \in \mathbb{C}^{ML}$.

Combining all $\mathbf{h}(n)$'s for $n = 0, 1, \dots, M - 1$ into one, higher dimensional channel vector, \mathbf{h} , can be expressed in terms of the lower dimensional BEM coefficient vector, \mathbf{c} , as

$$\mathbf{h} = \Phi\mathbf{c}, \quad (34)$$

where $\Phi = [\Phi^T(0), \Phi^T(1), \dots, \Phi^T(M-1)]^T \in \mathcal{R}^{ML \times DL}$. Finally, substituting (34) in (33), we obtain the reduced parameter observation equation as

$$\begin{aligned} \hat{\mathbf{H}} &= \text{diag}\{\hat{\mathbf{F}}(0), \hat{\mathbf{F}}(1), \dots, \hat{\mathbf{F}}(M-1)\} \Phi\mathbf{c} \\ &= \Pi\mathbf{c}. \end{aligned} \quad (35)$$

where $\Pi \triangleq \text{diag}\{\hat{\mathbf{F}}(0), \hat{\mathbf{F}}(1), \dots, \hat{\mathbf{F}}(M-1)\}\Phi$. Note that given K , M as well as delay and Doppler rate estimates, $\hat{\mathbf{F}}$ and Φ are fixed matrices that can be computed and stored in advance. Hence, the least-square (LS) solution for \mathbf{c} is obtained from (35) as,

$$\hat{\mathbf{c}} = (\Pi^\dagger\Pi)^{-1}\Pi^\dagger\hat{\mathbf{H}}. \quad (36)$$

Finally, given the estimated BEM coefficient vector, $\hat{\mathbf{c}}$, the sparse solution for the channel path gains, $\hat{\mathbf{h}}(n)$, that match the model $\hat{\mathbf{H}}(n)$ in whole OFDM frame can be obtained from (32) as

$$\hat{\mathbf{h}}(n) = \Phi(n)\hat{\mathbf{c}}, n = 0, 1, \dots, M - 1. \quad (37)$$

After the sparse channel impulse response, $\hat{\mathbf{h}}(n)$, has been obtained, the final refined estimated transfer function of the UWA channel is estimated by taking the discrete Fourier transform (DFT) after it is zero padded to the full length $K/2$ as

$$\hat{\mathbf{H}}(n) = \mathbb{F}_{K/2}\hat{\mathbf{h}}_Z(n), n = 0, 1, \dots, M - 1. \quad (38)$$

where $\mathbb{F}_{K/2}$ is the DFT matrix and $\hat{\mathbf{h}}_Z(n)$ is the zero padded version of $\hat{\mathbf{h}}(n)$. The final estimated transfer function of the UWA channel, $\hat{\mathbf{H}}(n)$, is used for data detection.

VI. EQUALIZATION AND DATA DETECTION

In order to operate the EM algorithm with good initial values that ensure lower number of iterations in the channel estimation process, P known data symbols (modulated on the pilots subcarriers) $\{d_{2k_p}(n), d_{2k_p+1}(n)\}$ with $k_p \in \{0, 1, \dots, K - 1, \}$ $p = 1, 2, \dots, P$, are evenly inserted into the K subcarriers in each OFDM block, known by the receiver. Hence, the data vectors $\mathbf{d}_e(n)$ and $\mathbf{d}_o(n)$ in (1) are superposition of the pilot vectors, $\mathbf{d}_{e,P}(n)$, $\mathbf{d}_{o,P}(n)$ and the unknown data vectors, $\mathbf{d}_{e,D}(n)$, $\mathbf{d}_{o,D}(n)$, transmitted from each of the transmit antenna, respectively, as $\mathbf{d}_e(n) = \mathbf{d}_{e,P}(n) + \mathbf{d}_{e,D}(n)$ and $\mathbf{d}_o(n) = \mathbf{d}_{o,P}(n) + \mathbf{d}_{o,D}(n)$. Note that, for $\times \in \{e, o\}$, $\mathbf{d}_{\times,P}(n)$, $\mathbf{d}_{\times,D}(n) \in \mathbb{C}^{K/2}$ contain nonzero components only at

the pilot positions and data positions, respectively. On the other hand, (4) can be expressed as

$$\begin{bmatrix} \mathbf{Y}_e^r(n) \\ \mathbf{Y}_o^{r*}(n) \end{bmatrix} = \begin{bmatrix} \hat{\mathcal{H}}_{\text{MAP}}^{1,r}(n) \hat{\mathcal{H}}_{\text{MAP}}^{2,r}(n) \\ \hat{\mathcal{H}}_{\text{MAP}}^{2,r\dagger}(n) - \hat{\mathcal{H}}_{\text{MAP}}^{1,r\dagger}(n) \end{bmatrix} \begin{bmatrix} \mathbf{d}_e(n) \\ \mathbf{d}_o(n) \end{bmatrix} + \begin{bmatrix} \mathbf{V}_e^r(n) \\ \mathbf{V}_o^r(n) \end{bmatrix}, \quad (39)$$

or in a more compact form

$$\tilde{\mathbf{Y}}^r(n) = \hat{\mathcal{H}}_{\text{MAP}}^r(n) \mathbf{d}(n) + \mathbf{V}^r(n), \quad (40)$$

where, for each $t = 1, 2$, and $r = 1, 2, \dots, n_R$, $\hat{\mathcal{H}}_{\text{MAP}}^{t,r}(n)$ is a $K/2 \times K/2$ diagonal matrix whose elements on the diagonal are the components of the vector $\mathbf{H}_{\text{MAP}}^{t,r}(n)$. Consequently, (40) can be expressed as

$$\begin{aligned} \mathbf{Z}_D^r(n) &\triangleq \tilde{\mathbf{Y}}^r(n) - \hat{\mathcal{H}}_{\text{MAP}}^r(n) \mathbf{d}_P(n) \\ &= \hat{\mathcal{H}}_{\text{MAP}}^r(n) \mathbf{d}_D(n) + \mathbf{V}^r(n), r = 1, 2, \dots, n_R, \end{aligned} \quad (41)$$

where

$$\hat{\mathcal{H}}_{\text{MAP}}^r(n) \triangleq \begin{bmatrix} \hat{\mathcal{H}}_{\text{MAP}}^{1,r}(n) \hat{\mathcal{H}}_{\text{MAP}}^{2,r}(n) \\ \hat{\mathcal{H}}_{\text{MAP}}^{2,r\dagger}(n) - \hat{\mathcal{H}}_{\text{MAP}}^{1,r\dagger}(n) \end{bmatrix}.$$

Using the Alamouti coding combining scheme [21], the following K -dimensional combined signal, that are sent to a minimum mean-square equalizer (MMSE) for final data detection, is constructed:

$$\mathbf{z}_D(n) \equiv \hat{\mathbb{H}}_{\text{MAP}}(n) \mathbf{z}_D(n) \in \mathcal{C}^K \quad (42)$$

where $\hat{\mathbb{H}}_{\text{MAP}}(n) = [\hat{\mathcal{H}}_{\text{MAP}}^1(n), \hat{\mathcal{H}}_{\text{MAP}}^2(n), \dots, \hat{\mathcal{H}}_{\text{MAP}}^{n_R}(n)] \in \mathcal{C}^{K \times n_R K}$, and $\mathbf{z}_D(n) \triangleq [\mathbf{z}_D^{1,T}(n), \mathbf{z}_D^{2,T}(n), \dots, \mathbf{z}_D^{n_R,T}(n)]^T \in \mathcal{C}^{n_R K \times 1}$. Substituting (41) in (42) yields

$$\mathbf{z}_D(n) = \mathbf{C}(n) \mathbf{d}_D(n) + \mathbf{N}(n) \quad (43)$$

where $\mathbf{C}(n)$ is a $K \times K$ positive definite diagonal matrix, determined from $\mathbf{C}(n) = \sum_{r=1}^{n_R} \|\hat{\mathcal{H}}_{\text{MAP}}^r(n)\|_F^2$, and $\mathbf{N}(n)$ is the resulting additive white Gaussian noise. Consequently, data symbols transmitted over even and odd OFDM subcarriers, namely, $\mathbf{d}_{e,D}(n)$, $\mathbf{d}_{o,D}(n)$, are detected by the decoupled observed equations given by (43). Hence, the detection is reduced to the case of single transmitter-receiver configuration with substantially less computational complexity. For $n = 0, 1, \dots, M-1$, the data detection operation is carried out using the minimum mean-square error (MMSE) equalizer as

$$\begin{aligned} \hat{\mathbf{d}}_{e,D}(n) \\ = \mathcal{D}et \left\{ \mathbf{C}_{11}^\dagger(n) \left(\mathbf{C}_{11}(n) \mathbf{C}_{11}^\dagger(n) + \zeta^{-1} \mathbf{I}_{K/2} \right)^{-1} \mathbf{z}_{e,D}(n) \right\}, \end{aligned} \quad (44)$$

$$\begin{aligned} \hat{\mathbf{d}}_{o,D}(n) \\ = \mathcal{D}et \left\{ \mathbf{C}_{22}^\dagger(n) \left(\mathbf{C}_{22}(n) \mathbf{C}_{22}^\dagger(n) + \zeta^{-1} \mathbf{I}_{K/2} \right)^{-1} \mathbf{z}_{o,D}(n) \right\}, \end{aligned} \quad (45)$$

where $\mathcal{D}et\{\cdot\}$ represents hard detection for the M -ary quadrature amplitude modulation (QAM) or phase-shift keying (PSK) data symbols. $\mathbf{z}_D(n) = [\mathbf{z}_{e,D}^T(n), \mathbf{z}_{o,D}^T(n)]^T$ and $\mathbf{C}_{11}(n)$ and $\mathbf{C}_{22}(n)$ are the diagonal elements of $\mathbf{C}(n)$ and ζ is the SNR. Note that as can be seen from (44) and (45) a diversity order of $2n_R$ is gained by the proposed scheme.

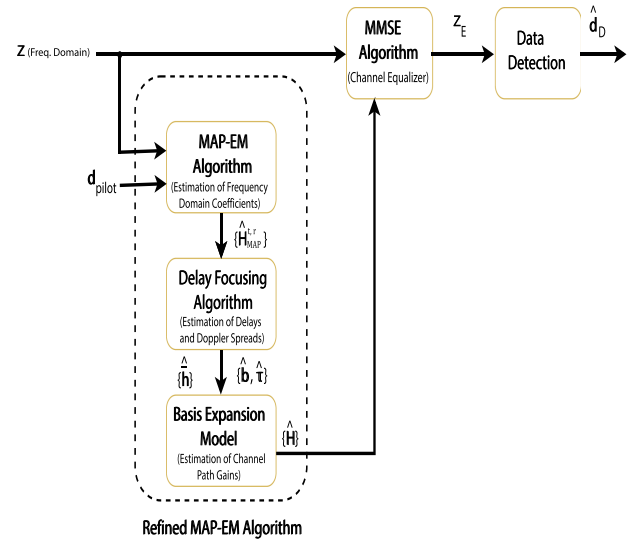


Fig. 2. Block diagram of the proposed channel estimation and equalization algorithm.

A complete block diagram of the channel estimation and equalization algorithm is given in Fig. 2.

VII. COMPUTER SIMULATIONS AND COMPUTATIONAL COMPLEXITY

In this section, we discuss the computational complexity and show the performance of our algorithm that takes into consideration the sparsity feature of the UWA channel. We evaluate the proposed approach in terms of the symbol error rate (SER) and the average mean square error (MSE). In addition, the minimum mean-square error (MMSE) equalizer is chosen for data detection, as explained in the previous section. The sparse UWA channels for computer simulations are first generated according to the channel model described in Sec. III. Subsequently, the UWA channel impulse response is acquired through VirTEX software [29] using the synthetic data obtained for Sapanca Lake in Turkey for further simulation studies.

A. Computational Complexity

Table I presents the computational complexity of the proposed algorithm. The implementation of the Alamouti MAP-EM algorithm in the frequency domain, including the initialization step requires approximately $(n_R M L_{CP} (9K + 8P))$ complex-multiplications (CMs) and $n_R M L_{CP} (8(K-1) + 5P)$ complex-additions (CAs). Note that L_{CP} appears in the computation due to the fact that the $(K/2 \times K/2)$ matrix in

(16) has the form as $\Xi^{-1} \mathbf{U}^\dagger = [A_{K/2 \times L_{CP}} \mid \mathbf{0}_{K/2 \times (K/2 - L_{CP})}]$.

Also, the SVD of the $(K/2 \times K/2)$ frequency-domain channel auto-correlation function is precomputed. Therefore, an iteration step of the MAP-EM only requires a multiplication of a precomputed matrix obtained from the precomputed SVD. The computational complexity of the time-domain refinement including the estimation of the channel Doppler spreads, the channel delays and the complex channel path gains, is approximately $(2 * n_R * M * (K + L * N_\tau * N_b))$ CMs and $2n_R * M * (K - 1 + L * M * (K + L * N_\tau * N_b))$ CAs.

TABLE I
COMPUTATIONAL COMPLEXITY DETAILS

ALAMOUTI CHANNEL ESTIMATION ALGORITHM IN THE FREQUENCY DOMAIN			
MAP-EM ALGORITHM INITIALIZATION			
Eq. No	Variable	CMs	CAs
(20)	$\mathbf{G}^{t,r(0)}(n)$	$\approx 8n_R * P * M$	$\approx 2 * n_R * M * (5 * P - 2)$
MAP-EM ALGORITHM (q)th ITERATION			
(15)	$\mathbf{G}^{t,r(q)}(n)$	$\approx 2 * n_R * M * L_{CP}(9K/2)$	$\approx 2 * n_R * M * L_{CP}(8 * K - 6)$
REFINED CHANNEL ESTIMATION ALGORITHM IN THE TIME DOMAIN			
(27)	$\Psi_q^{t,r}(n)$	$2n_R * M * K$	$2n_R * M * (K - 1)$
Alg. 1	$\{\hat{q}_\ell, \hat{b}_\ell\}$	$\approx 2n_R * L * M * N_b * N_\tau$	$\approx 2n_R * L * M * N_b * N_\tau$
EQUALIZATION AND DETECTION ALGORITHM			
(41)	$\mathbf{Z}_D^r(n)$	$\approx 4 * n_R * M * K$	$\approx 4 * n_R * M * (K - 1)$
(42)	$\mathbf{z}_D^r(n)$	$\approx 3 * n_R * M * K$	$\approx 3 * n_R * M * (K - 1)$
(44)	$\mathbf{C}_{ii}^{r\dagger}(n)(\mathbf{C}_{ii}^r(n)\mathbf{C}_{ii}^{r\dagger}(n) + \gamma^{-1}\mathbf{I}_{K/2})^{-1}$	$\approx 4 * n_R * M * K$	$\approx n_R * M * (3 * K - 4)$
(44)	$\hat{\mathbf{d}}_{e,D}^r(n), \hat{\mathbf{d}}_{o,D}^r(n)$	$\approx n_R * M * K$	$n_R * M * (K - 1)$

$N_\tau * N_b$) CAs. The computation of the equalizer output as well as the Alamouti-based data detection require approximately $(12 * N_\tau * M * K)$ CMs and $(n_r * M * (11 * K - 12))$ CAs. Finally, Table I shows that the computational complexity per one iteration of a complete Alamouti MAP-EM channel estimation, equalization and detection algorithms is approximately $(n_R * M * (K * (9 * L_{CP} + 14) + 8 * P + 2 * LN_\tau N_b))$ CMs and $(n_R * M * (K * (L_{CP} + 15) - 30 + 2 * LN_\tau N_b))$ CAs. Consequently, the complexity of the algorithm is of order $\mathcal{O}(K * L_{CP})$ per EM iteration.

B. Generation of UWA Channels for Computer Simulations

We now present the main approach to generate the sparse UWA channel for our computer simulations. Subsequently, we obtained the UWA channel impulse response examples through VirTEX software using the real data for Sapanca Lake in Turkey. The channel is generated according to (7) and (8), where initial values for the path gains $h_\ell^{t,r}(0)$ and the delays $\tilde{\tau}_\ell^t(0)$ are obtained using VirTEX simulations. Following the work presented in [23], the time-varying channel delays, $\tilde{\tau}_{\ell,i}^t$, were generated from (7). In order to be able to model more realistic UWA channels in this model, we also assume that Doppler scaling factors, b_ℓ^t 's, are path dependent, each generated from $[-b_{\max}, b_{\max}]$ with uniform distribution. This assumption is opposed to the approach adopted in [8] which considers same Doppler scaling factors for each path. To capture the motion effect within the scattering field, we have fitted nicely our ACF model, obtained in Sec. III, to an AR-1 model. Hence, we generate several UWA channels during our computer simulations as follows: In Appendix-A, the time ACF of the channel coefficients is shown to be

$$R_\ell(m) = \sigma_\ell^2 \text{sinc}(2f_c b_{\max} T_{\text{OFDM}} m), m = 0, 1, \dots, M - 1.$$

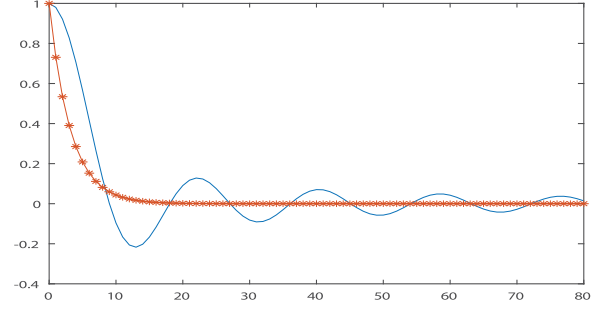


Fig. 3. ACF of the channel coefficients (dotted curve) and its approximation (solid curve).

TABLE II
OFDM AND SIMULATION PARAMETERS

channel bandwidth (BW)	4.883 kHz
carrier frequency (f_c)	10.580 kHz
OFDM symbol duration (T)	52.4 ms
number of OFDM subcarriers (K)	512
cyclic prefix duration (T_{CP})	12 ms
OFDM subcarrier spacing ($\Delta f := 1/T$)	19.075 Hz
modulation formats	QPSK
maximum Doppler spread (b_{\max})	$10^{-4} Hz$
Number of OFDM symbols in the frame M	25
pilot spacing (Δ_p)	2, 4, 6

As it can be seen in Fig. 3, that using the channel simulation parameters adopted in our work, the time ACF can be well approximated by $R_\ell(m) \approx \exp(-\pi B_d f_c T_{\text{OFDM}} m)$, where $B_d = 2b_{\max}$ is the effective Doppler bandwidth (Doppler spread) of the power spectral density (PSD) of $h_\ell^{t,r}(n)$. Hence, we can assume that the channel coefficients in (9) statistically equivalent to a first-order autoregressive process (AR-1).

$$h_\ell^{t,r}(n+1) = \alpha_\ell h_\ell^{t,r}(n) + w_\ell(n)$$

where $w(n) \sim \mathcal{CN}(0, \sigma_\ell^2(1 - \alpha_\ell^2))$ and $\alpha_\ell = e^{-\pi B_d f_c T_{\text{OFDM}} m}$.

Finally, the time-varying discrete channel autocorrelation coefficients, derived for this purpose in (10), are adopted to determine the SVD needed for the implementation of the MAP-EM based channel estimation algorithm.

Table II summarizes the main system parameters employed in our computer simulations. Transmission is implemented by frames, each consists of M OFDM symbols. Based on the overall signal observed within each frame, both UWA channel parameters are estimated and transmitted data is detected. We assume an equally spaced pilot subcarriers (comb-type pilot structure). Note that the pilot design and the optimal number of pilot subcarriers for UWA channels that experience high Doppler shift is beyond the scope of the current work. Also, in real UWAC system applications, the transceiver pair utilizes channel coding techniques which lower the amount of error at the receiver. In this work, however, we consider an uncoded OFDM-based UWAC system to illustrate the performance of the proposed approach.

C. Computer Simulations

The computer simulation results are presented in this subsection. These results assess the performance of the proposed sparse channel estimation algorithm.

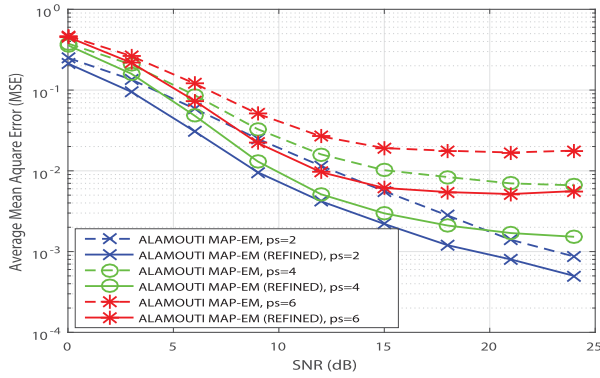


Fig. 4. MSE vs. SNR performance of the refined MAP-EM for different pilot spacing with $n_R = 1$, $b_{max} = 10^{-4}$, $K = 512$, and QPSK signaling.

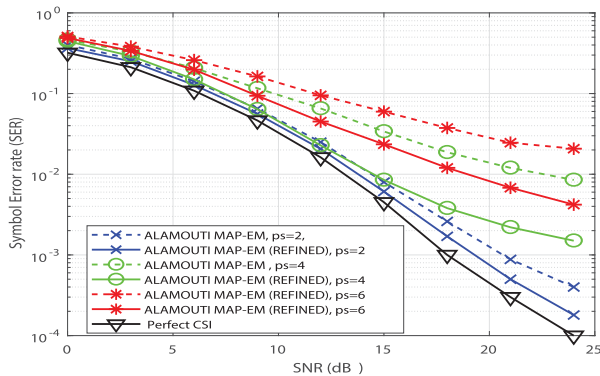


Fig. 5. SER vs. SNR performance of the refined MAP-EM for different pilot spacing with $n_R = 1$, $b_{max} = 10^{-4}$, $K = 512$, and QPSK signaling.

Assuming one receiving antenna ($n_R = 1$), Figs. 4 and 5 demonstrate the average mean square error (MSE) and the symbol error rate (SER), respectively, with refinement in time domain.

The average SNR is defined as $E\{|H^{t,r}k(n)|^2 A\{|d_k|^2/\sigma^2\}\}$ where σ^2 is the variance of the complex additive white Gaussian noise. Path gains are assumed to obey a Rayleigh fading model. MSE is defined as the norm of the difference between the vectors \mathbf{G} and $\hat{\mathbf{G}}_{MAP}$, representing the true and the estimated values of the channel parameters, respectively. The MSE and SER performances before and after the time-domain refinement vs. SNR curves are shown with quadrature amplitude modulated (QAM) symbols and with Doppler spread $b_{max} = 10^{-4}$ for different pilot spacing. As seen from Figs. 4 and 5, the refinement performed after the channel estimation realized in the frequency domain has significant positive impact on improving the performances (MSE and SER) of the algorithm. Moreover, it can be also seen from these curves that the proposed algorithm can sufficiently handle a comb-type pilot spacing of $\Delta_p = 4$ and tolerate the Doppler spreads around $b_{max} = 10^{-4}$. However, the MSE and SER performances degrade rapidly as the pilot spacing increases for $\Delta_p > 4$. Note that, this is consistent with the theoretical results that there exist a minimum subcarrier spacing $\Delta_{p_{min}}$ between pilots given by $\Delta_{p_{min}} < BW/(2 * K)$. For $BW = 4883$ Hz and $K = 512$, adopted in our computer simulations, $\Delta_{p_{min}} = 4.7686$. Note that in UWA communications, the channel introduces a high Doppler spread causing an

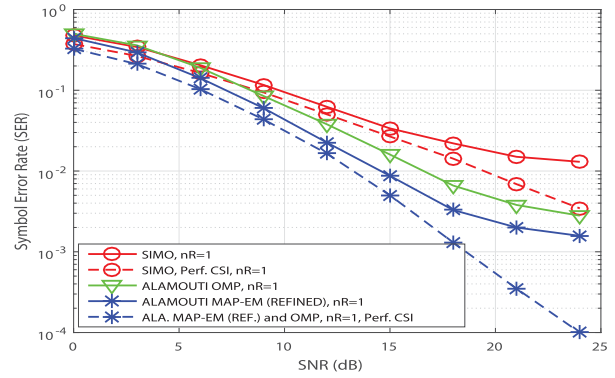


Fig. 6. SER vs. SNR Performance comparison between SIMO, SF Alamouti MAP-EM, and OMP for $\Delta_p = 4$, $K = 512$, $b_{max} = 10^{-4}$, and $n_R = 1$ with QPSK signaling.

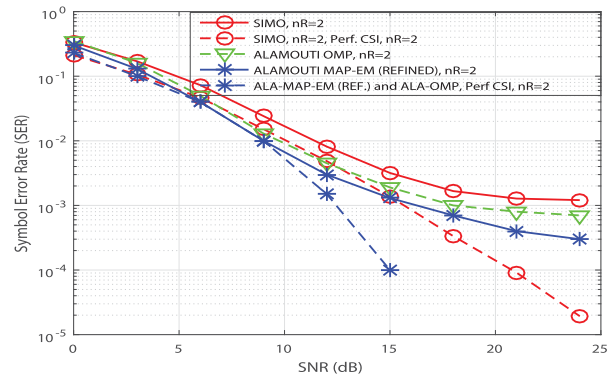


Fig. 7. SER vs. SNR Performance comparison between SIMO, SF Alamouti MAP-EM, and OMP for $\Delta_p = 4$, $K = 512$, $b_{max} = 10^{-4}$, and $n_R = 2$ with QPSK signaling.

observable error floor. As can be seen from Fig. 5 that even the UWA channel is estimated perfectly, the SER performance of the UWA communications systems would yield some amount of error floor depending on the Doppler spread.

Assuming a residual Doppler spread $b_{max} = 10^{-4}$, a pilot spacing $\Delta_p = 4$ and QPSK signaling format, Figs. 6 and 7, illustrate the SER vs. SNR performances with $n_R = 1$ and $n_R = 2$ receive antennas, respectively. These figures show the performance of the Alamouti space frequency orthogonal matching pursuit (OMP) channel estimation algorithm and the proposed refined MAP-EM algorithms. Fig. 7 utilizes a single-input multiple output (SIMO) system. The purpose of this figure is to reflect a benchmark case of the proposed approach by, by employing the refined MAP-EM channel estimation algorithm, having the same average transmit power and maximum ration combining detection scheme at the receiver. As depicted in Figs. 6 and 7, the refined MAP-EM algorithm has best SER vs. SNR performance and uniformly outperforms the Alamouti OMP estimator as well as SIMO channel estimator. For instance, the SER performances, at the SNR region of 20-25 dB, of the MAP-EM algorithm outperforms the Alamouti-OMP algorithm with about 4-5 dB. This is, however, due to the utilization of the prior information of the Rayleigh distributed channel gains in the MAP-EM algorithm. Note that, these gains are reached with a computationally more efficient way provided by the proposed algorithm.

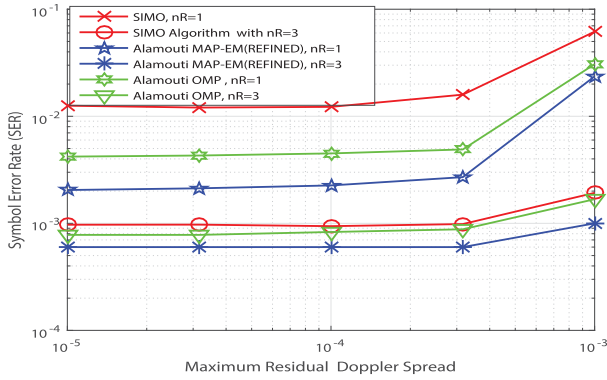


Fig. 8. SER vs. Residual Doppler Spread performance comparison between SIMO, SF Alamouti MAP-EM and OMP for SNR 20 dB. $K = 512$, $\Delta_p = 4$.

Assuming pilot spacing $\Delta_p = 4$ and QPSK signaling, Fig. 8 shows a comparison in the SER performance of the proposed refined MAP-EM and the OMP based channel estimation algorithms for different residual Doppler shifts. For benchmarking purposes, this figure also presents different number of receiving antennas $n_R = 1, 3$. As illustrated, the proposed approach with its sparsity feature can provide a lower error symbol rate in presence of Doppler shifts of order 5×10^{-4} Hz. Note that, beyond this value, $b_{\max} = 10^{-4}$ Hz, it is considered as a severe Doppler shift. However, the SER performance of the MAP-EM algorithm again uniformly outperforms the channel estimation based on both the OMP and SIMO for the number of receiving antennas $n_R = 1$ and $n_R = 3$. In addition, Fig. 8 shows that the SER performance of the refined MAP-EM algorithm is more pronounced when $n_R = 1$ and tolerates higher Doppler frequencies than OMP and SIMO.

D. Semi Experimental Simulation Results

In this subsection, we investigate the performance of the proposed approach over Sapanca Lake in Turkey using synthetic channels generated by the VirTEX acoustic toolbox [29]. VirTEX is known for its capability of reflecting the precise characteristics of an underwater region. It operates by post-processing the outputs produced by the BELLHOP [28] and computes the time series and the effects of the multipath propagation and the difference of Doppler shifts of each path from the ray theory analysis. These effects are introduced by the environmental movement in the underwater region. Mainly, the transceiver relative movement as well as the fluctuations in the sea. The lake is approximately 5 km wide and 16 km long. It is located at a latitude of 40.7163 and a longitude of 30.2628 with fresh water. The deepest point of the lake is ~ 53 m. The communication range chosen for this experiment is 5 km and the corresponding transceivers are considered to be placed at 50 meters of depth. Table III contains a summary of the simulation parameters.

Using the ray tracing technique implemented by VirTEX for the given underwater environment, the direct path and the reflected paths of the acoustic waves with significant power at the receiver (non-zero paths) between the source and the destination are generated. This VirTEX outputs a deterministic raw channel impulse response which is then normalized and augmented by introducing one of the several fading models encountered in

TABLE III
CHANNEL AND SIMULATION PARAMETERS FOR SAPANCA LAKE

channel bandwidth (BW)	4 kHz
carrier frequency (f_c)	16 kHz
OFDM symbol duration (T)	128 ms
number of OFDM subcarriers (K)	512
cyclic prefix duration (T_{CP})	30 ms
OFDM subcarrier spacing ($\Delta f := 1/T$)	7.81 Hz
channel Rician factor κ_ℓ	10
maximum Doppler spread (b_{\max})	5×10^{-5} Hz
pilot spacing (Δ_p)	2, 4, 6
modulation formats	QPSK
Number of OFDM symbols in the frame M	30

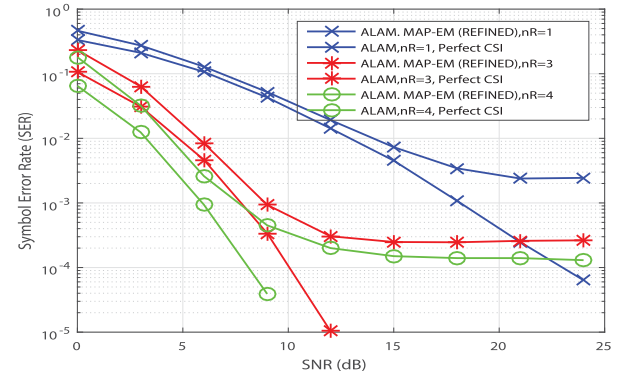


Fig. 9. SER vs. SNR performance of the Alamouti refined MAP-EM algorithm for different number of receiving antennas with $b_{\max} = 10^{-4}$, $K = 512$, and QPSK signaling.

UWA communications such as Rayleigh, Rician as well as Log-Normal. However, due to the semi-steady state of the water motion in the lake, the Doppler effect would arise. For the given environment, using the ray tracing technique implemented by VirTEX, the direct path and the reflected paths of the acoustic waves with significant power at the receiver (non-zero paths) between the source and destination are generated. As explained in [13] in detail, the CIR that considers the effective (non-zero) taps, L , is obtained after applying clustering and shareholding processes on the channel taps. However, the unnormalized delay of the acoustical waves is expected to be within 3.43 s. This assumption is based on the communication range (5 km) and the average sound speed in the lake ~ 1.455 km/s. The resulting delay spread is ~ 28 ms with 3 to 4 significant paths sparse channel.

Note that, to reflect the presence of the channel fading of the lake with the VirTEX toolbox, the statistical prediction model (SPM), proposed by [30] was adopted.

Considering the carrier frequency 16 kHz, we implement the SPM by varying the wave height and wavelength parameters related to the surface wave activity. In addition, we perform random slow variations of the positions of the transceivers. That is, according to the water movement of the Sapanca Lake during the winter season, the surface wave height is assumed to be between (0.5-1) m with steps 7.5 cm and the surface wavelength between (25-50)m in steps 1 m. Hence, the pdf estimated by the SPM fits in a Rician distribution with a Rician factor of $\kappa_\ell \approx 10$ for all channel paths. Consequently, this Rician factor value is used in our computer simulations.

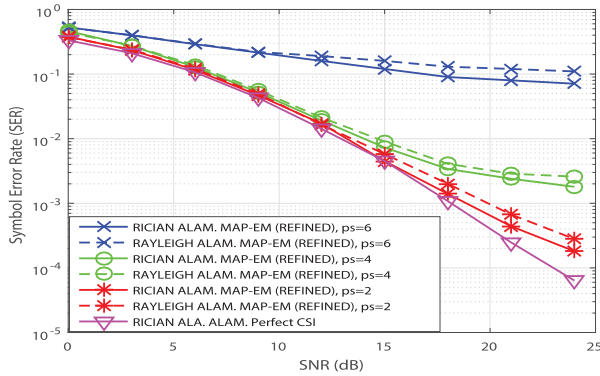


Fig. 10. Mismatch in SER vs. SNR performance between Rayleigh and Rician fading for $\Delta_p = 4$, $n_r = 1$, $b_{\max} = 10^{-4}$, and QPSK signaling.

In Fig. 9, a SER performance comparison of the Alamouti MAP-EM and the refined MAP-EM algorithms is investigated. Assuming $n_r = 1, 3, 4$ receive antennas, a maximum Doppler shift $b_{\max} = 10^{-4}$, pilot spacing $\Delta_p = 4$ and QPSK signaling as a function of SNR. The number of OFDM subcarriers is selected as $K = 512$. It can be seen from these curves that SER performance of the system improves substantially and excellent SER values are reached for $n_r = 4$. However, our extensive computer simulations have shown that the gain in SER performance became quite limited beyond $n_r > 5$.

Fig. 10 investigates the mismatch analysis. It shows the performance of our proposed channel estimation in the presence of different fading models. Whereas our approach is constructed based on Rayleigh model. Consequently, in such a mismatch scenario, the error performance of the channel estimation algorithm is degraded. This is mainly due to the fact that prior information employed in designing the Alamouti MAP-EM algorithm changes depending on the fading model. For example, the Rician fading has the same complex Gaussian distribution as Rayleigh fading but with a non-zero mean. Similarly, the Nakagami and the log-normal fading models are no longer Gaussian, which violates the Gaussian assumption, employed in our approach, of the prior distribution. In Fig. (10), the SER performance is analyzed, in such mismatched situation, in Rician fading when the Rayleigh fading is the correct model. It was shown earlier that the Rician fading is quite fitted in the Sapanca Lake with Rician factor equal to 10 [13].

The residual Doppler, in the simulations, is drawn uniformly from $[-b_{\max}, b_{\max}]$ with $b_{\max} = 10^{-4}$. The other simulation parameters are chosen according to Table II. As can be seen from the depicted curves shown in this figure, there is no substantial discrepancies in SER performance between two fading models. That is the Alamouti MAP-EM algorithm designed for the Rayleigh fading prior information is quite robust against Rician fading.

VIII. CONCLUSION

This paper has presented a sparse channel estimation algorithm for underwater communication systems that considers transmit diversity in the form of two transmitters and multiple receivers with Alamouti's space-frequency block coding with OFDM. In order to estimate the underwater complex channel

coefficients at each OFDM subcarrier, the proposed non-data-aided iterative approach utilizes the Expectation Maximization method, which guarantees convergence to a true maximum *a posteriori* probability estimate. However, the approach takes into account the sparseness feature of the UWA channel. Based on that, the estimated sparse solution of the channel impulse response that best matches the frequency-domain channel estimates obtained during the first phase of the estimation process is refined and the estimation performance was greatly improved. Sparse channel path delays and Doppler scaling factors are estimated by a novel technique called *delay focusing*. After that, slow time-varying, complex-valued channel path gains are estimated using a basis expansion model (BEM) based on the discrete Legendre polynomial expansion. The complete computational complexity of the proposed approach was shown to be $\sim O(K L_{CP})$ per EM iteration, proving that it is computationally very efficient. Finally, the computer simulations presented have shown excellent MSE and SER performances, especially when using multiple receiving antennas at the receiver. It was also observed through the mismatch analysis that the algorithm's error performance was quite robust against some different fading models.

APPENDIX A

DERIVATION OF THE ACF AND PSD OF THE CHANNEL

Using the delay model $\delta\tau_{\ell,i}^t(n) = \delta\tau_{\ell,i}(n) - b_{\ell}^t n T_{\text{OFDM}}$ in (7) and assuming path gains on each path remain constant over one OFDM symbol and vary independently from the symbol to symbol, that is $A_{\ell,i}^{t,r}(n) \approx A_{\ell,i}^{t,r}$, (9) can be expressed as

$$h_{\ell}^{t,r}(n) = h_{\ell}^{t,r} \exp(j2\pi f_c b_{\ell}^t n T_{\text{OFDM}}),$$

where $h_{\ell}^{t,r} = \sum_i A_{\ell,i}^{t,r} \exp(j2\pi f_c \delta\tau_{\ell,i}^{t,r})$. Assuming the components in the summation are independent and identically distributed, by the central limit theorem, the channel coefficients, $h_{\ell}^{t,r}$, are close to complex Gaussian random variables with variance σ_{ℓ}^2 and mean zero, assuming Rayleigh fading. Then the time correlation of the channel coefficients can be obtained as

$$\begin{aligned} R_{\ell}(m) &= E\{h_{\ell}^{t,r}(n+m)h_{\ell}^{t,r*}(n)\} \\ &= \sigma_{\ell}^2 E\{\exp(j2\pi f_c b_{\ell}^t m T_{\text{OFDM}})\}. \end{aligned} \quad (\text{A.1})$$

Since the path depending Doppler rates b_{ℓ} 's have uniform distribution in $[-b_{\max}, b_{\max}]$, taking expectation in (A.1) on this distribution yields

$$R_{\ell}(m) = \sigma_{\ell}^2 \text{sinc}(2f_c b_{\max} T_{\text{OFDM}} m), \quad m = 0, 1, \dots, M-1.$$

Finally the PSD of the UWA channel (channel's scattering function) for each path ℓ can be found as

$$\begin{aligned} S_{\ell}(\Omega) &= \sum_{m=0}^{M-1} R_{\ell}(m) e^{-j\Omega m} \\ &= \sigma_{\ell}^2 \sum_{m=0}^{M-1} \text{sinc}(2f_c b_{\max} T_{\text{OFDM}} m) e^{-j\Omega m}. \end{aligned}$$

where $\Omega = 2\pi f T_s$. Note that the summation above cannot be taken analytically. However, to get more inside of the PSD, $S_{\ell}(\Omega)$ can be expressed in a more convenient form as follows. Expanding $\exp(-j\Omega m)$ around the carrier frequency

$\Omega_c = 2\pi f_c T_s$, and substituting in the PSD expression above we have

$$S_\ell(\Omega) = \sum_{k=0}^{\infty} a_k \frac{(-j)^k (\Omega - \Omega_c)^k}{k!},$$

where

$$a_k = \sum_{m=0}^{M-1} m^k R_\ell(m) e^{-j\Omega_c m}.$$

It can be easily shown that $a_k = (-1)^k \frac{\partial^k S_\ell(\Omega)}{\partial \Omega^k} \big|_{\Omega=\Omega_c}$. Our computer simulation shows that $S_\ell(\Omega)$ is sufficiently smooth within the band $|\Omega - \Omega_c| \leq 2\pi b_{\max} T_s$ and the ratio $|m_k/m_0|$ vanishes rapidly as k gets larger. Hence only few terms are sufficient for computation of $S_\ell(\Omega)$.

APPENDIX B DERIVATION OF (10)

In this appendix, a proof of 10 is provided. For notational simplicity, we omit the symbol (t, r) in the derivations. The frequency domain auto-correlation function (ACF) is defined as $\mathbf{r}_n(m) = \{H_k(n)H_{k+m}^*(n)\}$ for each time index $n = 0, 1, \dots, M-1$. From Eqs. 7 and 8, and taking into account that $h_\ell^{t,r}(n)$ and $h_{\ell'}^{t,r}(n)$ are independent for different channel paths $\ell \neq \ell' \in \{0, 1, \dots, L-1\}$, it follows that

$$\begin{aligned} & \mathbf{r}_n(u) \\ &= E \left\{ \sum_{\ell} |h_\ell(n)|^2 \exp\left(-j \frac{2\pi u \tilde{\tau}_\ell^{t,r}}{K}\right) \exp\left(j \frac{2\pi u b_\ell^t T_{\text{OFDM}}}{K}\right) \right\}. \end{aligned}$$

Since, the channel coefficients and the residual Doppler rate are statistically independent, we have

$$\begin{aligned} \mathbf{r}_n(u) &= \sum_{\ell} E \left\{ |h_\ell(n)|^2 \exp\left(-j \frac{2\pi u \tilde{\tau}_\ell^{t,r}}{K}\right) \right\} \\ & \times E \left\{ \exp\left(j \frac{2\pi u b_\ell^t T_{\text{OFDM}}}{K}\right) \right\}. \end{aligned} \quad (\text{B.1})$$

Taking into account that b_ℓ^t 's are uniformly distributed over $[-b_{\max}, b_{\max}]$, the second expectation in the above expression can be taken as

$$\mathbf{r}_2 \triangleq E \left\{ \exp\left(j \frac{2\pi u b_\ell^t T_{\text{OFDM}}}{K}\right) \right\} = \text{sinc}\left(\frac{2b_{\max} T_{\text{OFDM}} n u}{K}\right). \quad (\text{B.2})$$

On the other hand, substituting $P_D(\tilde{\tau}_\ell^t) = |h_\ell(n)|^2$ in (B.1) the first expectation becomes

$$\mathbf{r}_1 \triangleq E \left\{ P_D(\tilde{\tau}_\ell^{t,r}) \exp\left(-j \frac{2\pi u \tilde{\tau}_\ell^{t,r}}{K}\right) \right\} \quad (\text{B.3})$$

where, $P_D(\tilde{\tau}_\ell^{t,r}) = C \exp(-\tilde{\tau}_\ell^{t,r}/\tau_{\text{rms}})$ is the channel power delay profile having an exponential decay model and C is the normalizing constant. Then \mathbf{r}_1 can be expressed as

$$\mathbf{r}_1 = \int f_{\tilde{\tau}_\ell^{t,r}}(\tau) P_D(\tau) e^{-j2\pi\tau u/K} d\tau$$

where $f_{\tilde{\tau}_\ell^{t,r}}(\tau)$ is the probability density function of $\tilde{\tau}_\ell^{t,r}$. For each independent channel paths delay, $f_{\tilde{\tau}_\ell^{t,r}}(\tau)$ has a uniform distribution over the duration of the cyclic prefix T_{CP} . Substituting $f_{\tilde{\tau}_\ell^{t,r}}(\tau)$, having an uniform distribution in \mathbf{r}_1 , and

normalizing it to unity yields

$$\mathbf{r}_1 = \frac{1 - e^{-L_{\text{CP}} \left(\frac{1}{\tau_{\text{rms}}} + 2\pi j u / K \right)}}{\tau_{\text{rms}} \left(1 - e^{-L_{\text{CP}} / \tau_{\text{rms}}} \right) \left(\frac{1}{\tau_{\text{rms}}} + j 2\pi \frac{u}{K} \right)}.$$

Finally the final analytical frequency-domain ACF at each time index n is obtained as $\mathbf{r}_n(u) = \mathbf{r}_1 \times \mathbf{r}_2$, which is the expression given by 10.

APPENDIX C DERIVATION OF (15)

The term $\log p(\mathbf{Y}^r, \mathcal{D}, \mathbf{G}^r)$ in (14) can be written as

$$\begin{aligned} \log p(\mathbf{Y}^r, \mathcal{D}, \mathbf{G}^r) &\sim p(\mathcal{D}, \mathbf{G}^r) \\ &+ \log p(\mathbf{Y}^r | \mathcal{D}, \mathbf{G}^r) + \log p(\mathbf{G}^r). \end{aligned} \quad (\text{C.1})$$

The first term in (C.1) is constant since \mathcal{D} and \mathbf{G}^r are independent of each other and the fact that the data sequences, \mathcal{D} , have an equal *a priori* probability. In addition, since the noise samples are independent, from (2) and (12), the second and third terms in (C.1), can be expressed as

$$\begin{aligned} \log p(\mathbf{Y}^r | \mathcal{D}, \mathbf{G}^r) &\sim -\frac{1}{\sigma^2} \left(\mathbf{Y}_e^r - \mathcal{D}_e \mathbf{U} \mathbf{G}^{1,r} - \mathcal{D}_o \mathbf{U} \mathbf{G}^{2,r} \right)^\dagger \\ & \times \left(\mathbf{Y}_e^r - \mathcal{D}_e \mathbf{U} \mathbf{G}^{1,r} - \mathcal{D}_o \mathbf{U} \mathbf{G}^{2,r} \right) \\ & - \frac{1}{\sigma^2} \left(\mathbf{Y}_o^r + \mathcal{D}_o^\dagger \mathbf{U} \mathbf{G}^{1,r} - \mathcal{D}_e^\dagger \mathbf{U} \mathbf{G}^{2,r} \right)^\dagger \\ & \times \left(\mathbf{Y}_o^r + \mathcal{D}_o^\dagger \mathbf{U} \mathbf{G}^{1,r} - \mathcal{D}_e^\dagger \mathbf{U} \mathbf{G}^{2,r} \right), \\ \log p(\mathbf{G}^r) &\sim -\mathbf{G}^{1,r\dagger} \mathbf{\Lambda}^{-1} \mathbf{G}^{1,r} - \mathbf{G}^{2,r\dagger} \mathbf{\Lambda}^{-1} \mathbf{G}^{2,r}. \end{aligned} \quad (\text{C.2})$$

Taking derivatives in (14) with respect to $\mathbf{G}^{1,r}$ and $\mathbf{G}^{2,r}$ and by equating the resulting equations to zero, we can obtain

$$\begin{aligned} \frac{\partial Q}{\partial \mathbf{G}^{1,r}} &= \sum_{\mathcal{D}} p(\mathbf{Y}^r, \mathcal{D}, \mathbf{G}^{(q)}) \left[\frac{1}{\sigma^2} \mathbf{U}^\dagger (\mathcal{D}_e^\dagger \mathbf{Y}_e^r - \mathcal{D}_o \mathbf{Y}_o^r) \right. \\ & \left. - \left(\frac{1}{\sigma^2} \mathbf{U}^\dagger (\|\mathcal{D}_e\|_F^2 + \|\mathcal{D}_o\|_F^2) \mathbf{U} - \mathbf{\Lambda}^{-1} \right) \mathbf{G}^{1,r} \right] = 0, \\ \frac{\partial Q}{\partial \mathbf{G}^{2,r}} &= \sum_{\mathcal{D}} p(\mathbf{Y}^r, \mathcal{D}, \mathbf{G}^{(q)}) \left[\frac{1}{\sigma^2} \mathbf{U}^\dagger (\mathcal{D}_o^\dagger \mathbf{Y}_e^r + \mathcal{D}_e \mathbf{Y}_o^r) \right. \\ & \left. - \left(\frac{1}{\sigma^2} \mathbf{U}^\dagger (\|\mathcal{D}_e\|_F^2 + \|\mathcal{D}_o\|_F^2) \mathbf{U} - \mathbf{\Lambda}^{-1} \right) \mathbf{G}^{2,r} \right] = 0 \end{aligned} \quad (\text{C.3})$$

Replacing $p(\mathbf{Y}^r, \mathcal{D}, \mathbf{G}^{(q)})$ by $p(\mathcal{D} | \mathbf{Y}^r, \mathbf{G}^{(q)})$ without violating the equalities in (C.3), we can define the conditional probabilities as

$$\begin{aligned} \Gamma_{t,r}^{(q)}(k) &\triangleq \\ & \sum_{a_1} \sum_{a_2 \in \mathcal{S}_k} a_t P \left(d_{2k}(n) = a_1, d_{2k+1}(n) = a_2 | \mathbf{Y}^r, \mathbf{G}^{(q)} \right), \end{aligned}$$

$$\mathcal{R}_{t,r}^{(q)}(k) = \frac{\sum_{i=1}^{\sqrt{M}/2} \sum_{j=1}^{\sqrt{M}/2} (2i-1) e^{-\frac{(2i-1)^2 + (2j-1)^2}{\sigma^2}} \|\mathbf{G}^{r(q)}\|_F^2 \sinh\left(\frac{2}{\sigma^2} \frac{1}{\sqrt{P_{av}}} (2i-1) \Re\{Z_{t,r}^{(q)}(k)\}\right)}{\sum_{i=1}^{\sqrt{M}/2} \sum_{j=1}^{\sqrt{M}/2} e^{-\frac{(2i-1)^2 + (2j-1)^2}{\sigma^2}} \|\mathbf{G}^{t(q)}\|_F^2 \cosh\left(\frac{2}{\sigma^2} \frac{1}{\sqrt{P_{av}}} (2i-1) \Re\{Z_{t,r}^{(q)}(k)\}\right)}$$

$$\mathcal{Q}_{t,r}^{(q)}(k) = \frac{\sum_{i=1}^{\sqrt{M}/2} \sum_{j=1}^{\sqrt{M}/2} (2i-1) e^{-\frac{(2i-1)^2 + (2j-1)^2}{\sigma^2}} \|\mathbf{G}^{r(q)}\|_F^2 \sinh\left(\frac{2}{\sigma^2} \frac{1}{\sqrt{P_{av}}} (2j-1) \Im\{Z_{t,r}^{(q)}(k)\}\right)}{\sum_{i=1}^{\sqrt{M}/2} \sum_{j=1}^{\sqrt{M}/2} e^{-\frac{(2i-1)^2 + (2j-1)^2}{\sigma^2}} \|\mathbf{G}^{r(q)}\|_F^2 \cosh\left(\frac{2}{\sigma^2} \frac{1}{\sqrt{P_{av}}} (2i-1) \Im\{Z_{t,r}^{(q)}(k)\}\right)}$$

$$\Upsilon_{t,r}^{(q)}(k) = \frac{\sum_{i=1}^{\sqrt{M}/2} \sum_{j=1}^{\sqrt{M}/2} \frac{((2i-1)^2 + (2j-1)^2)}{P_{av}} e^{-\frac{(2i-1)^2 + (2j-1)^2}{\sigma^2}} \|\mathbf{G}^{r(q)}\|_F^2 \cosh\left(\frac{2}{\sigma^2} \frac{1}{\sqrt{P_{av}}} (2i-1) \Re\{Z_{t,r}^{(q)}(k)\}\right)}{\sum_{i=1}^{\sqrt{M}/2} \sum_{j=1}^{\sqrt{M}/2} e^{-\frac{(2i-1)^2 + (2j-1)^2}{\sigma^2}} \|\mathbf{G}^{r(q)}\|_F^2 \cosh\left(\frac{2}{\sigma^2} \frac{1}{\sqrt{P_{av}}} (2i-1) \Re\{Z_{t,r}^{(q)}(k)\}\right)}$$

$$\Upsilon_{t,r}^{(q)}(k) \triangleq$$

$$\sum_{a_1} \sum_{a_2 \in \mathbf{S}_k} |a_t|^2 P \left(d_{2k}(n) \triangleq a_1, d_{2k+1}(n) = a_2 | \mathbf{Y}^r, \mathbf{G}^{(q)} \right),$$

and the $K/2 \times K/2$ diagonal matrices

$$\mathbf{\Gamma}_{t,r}^{(q)} = \text{diag} \left(\Gamma_{t,r}^{(q)}(0), \dots, \Gamma_{t,r}^{(q)} \left(\frac{K}{2} - 1 \right) \right),$$

$$\mathbf{\Upsilon}_{t,r}^{(q)} = \text{diag} \left(\Upsilon_{t,r}^{(q)}(0), \dots, \Upsilon_{t,r}^{(q)} \left(\frac{K}{2} - 1 \right) \right). \quad (\text{C.4})$$

The equations in (C.3) can then be expressed as

$$\mathbf{U}^\dagger \left(\mathbf{\Gamma}_{1,r}^{(q)\dagger} \mathbf{Y}_e^r - \mathbf{\Gamma}_{2,r}^{(q)} \mathbf{Y}_o^r \right)$$

$$= \left(\mathbf{U}^\dagger \left(\mathbf{\Upsilon}_{1,r}^{(q)} + \mathbf{\Upsilon}_{2,r}^{(q)} \right) \mathbf{U} + \sigma^2 \mathbf{\Lambda}^{-1,r} \right) \mathbf{G}^{1,r}$$

$$\mathbf{U}^\dagger \left(\mathbf{\Gamma}_{2,r}^{(q)\dagger} \mathbf{Y}_e^r + \mathbf{\Gamma}_{1,r}^{(q)} \mathbf{Y}_o^r \right)$$

$$= \left(\mathbf{U}^\dagger \left(\mathbf{\Upsilon}_{1,r}^{(q)} + \mathbf{\Upsilon}_{2,r}^{(q)} \right) \mathbf{U} + \sigma^2 \mathbf{\Lambda}^{-1} \right) \mathbf{G}^{2,r}$$

from which, the final expression for $\mathbf{G}^{t,r(q+1)}$, $t = 1, 2$, given by (16) easily follows.

APPENDIX D

$\mathbf{\Gamma}_{t,r}^{(q)}(k)$ AND $\mathbf{\Upsilon}_{t,r}^{(q)}(k)$ COMPUTATION FOR AN M -QAM SIGNAL CONSTELLATION

Let, for $t = 1, 2$, a_t represents the unit power square M -QAM signal point in two dimensions whose coordinates are chosen from the set $\mathcal{S} = \frac{1}{\sqrt{P_{av}}} \{\pm 1, \pm 3, \dots, \pm \sqrt{M} - 1\}$, where $P_{av} = \frac{2(M-1)}{3}$ is the average signal power. Since

$$\text{Prob} \left(d_{2k}(n) = a_1, d_{2k+1}(n) = a_2 | \mathbf{Y}^r, \mathbf{G}^{r(q)} \right)$$

$$\sim p \left(\mathbf{Y}^r | d_{2k}(n) = a_1, d_{2k+1}(n) = a_2, \mathbf{G}^{r(q)} \right),$$

from (C.2), and after some algebra, $\mathbf{\Gamma}_{t,r}^{(q)}(k)$ and $\mathbf{\Upsilon}_{t,r}^{(q)}(k)$ can be written as follows:

$$\mathbf{\Gamma}_{t,r}^{(q)}(k) = \frac{1}{\sqrt{P_{av}}} \left(\mathcal{R}_{t,r}^{(q)}(k) + j \mathcal{Q}_{t,r}^{(q)}(k) \right), \quad (\text{D.1})$$

where $\mathcal{R}_{t,r}^{(q)}(k)$ and $\mathcal{Q}_{t,r}^{(q)}(k)$ are shown at the top of the page.

Similarly from (C.4) it follows that $\Upsilon_{t,r}^{(q)}(k)$ is as shown at the top of the page, where $\|\mathbf{G}^{r(q)}\|_F^2 = \|\mathbf{G}^{1,r(q)}\|_F^2 + \|\mathbf{G}^{2,r(q)}\|_F^2$ and

$$Z_{1,r}^{(q)}(k) = \frac{1}{2} Y_{2k}^r(n) \sum_{m=0}^{K/2-1} u_m^*(k) G_{2m}^{t,r(q)*}(n)$$

$$+ Y_{2k+1}^{*,r}(n) \sum_{m=0}^{K/2-1} u_m(k) G_{2m+1}^{t,r(q)}(n),$$

$$Z_{2,r}^{(q)}(k) = \frac{1}{2} Y_{2k}^r(n) \sum_{m=0}^{K/2-1} u_m^*(k) G_{2m+1}^{t,r(q)*}(n)$$

$$- Y_{2k+1}^{*,r}(n) \sum_{m=0}^{K/2-1} u_m(k) G_{2m}^{t,r(q)}(n), \quad (\text{D.2})$$

with $k = 0, 1, \dots, K/2 - 1$ and $u_m(k)$ are the k th components of the eigenvectors \mathbf{u}_m , $m = 1, 2, \dots, K/2 - 1$, of the autocorrelation matrix \mathfrak{R} defined in Section IV.

REFERENCES

- [1] L. Liu, S. Zhou, and J. Cui, "Prospects and problems of wireless communications for underwater sensor networks," *Wireless Commun. Mobile Comput.*, vol. 8, no. 8, pp. 977–994, Oct. 2008.
- [2] A. Radosevic, T. Duman, J. Proakis, and M. Stojanovic, "Selective decision directed channel estimation for UWA OFDM systems," in *Proc. 49th Ann. Allerton Conf. Commun. Control Comput.*, 2011, pp. 647–653.
- [3] C. R. Berger, S. Zhou, J. Preisig, and P. Willett, "Sparse channel estimation for multicarrier underwater acoustic communication: From subspace methods to compressed sensing," *IEEE Trans. Signal Process.*, vol. 58, no. 3, pp. 1708–1721, Mar. 2010.
- [4] W. Li and J. C. Preisig, "Estimation of rapidly time-varying sparse channels," *IEEE J. Ocean. Eng.*, vol. 32, no. 4, pp. 927–939, Oct. 2007.
- [5] M. Stojanovic, "OFDM for underwater acoustic communications: Adaptive synchronization and sparse channel estimation," in *Proc. IEEE Int. Conf. Acoust. Speech Signal Process.*, 2008, pp. 5288–5291.
- [6] S. F. Mason, C. R. Berger, Z. Zhou, and P. Willett, "Detection, synchronization, and doppler scale estimation with multicarrier waveforms in underwater acoustic communication," *IEEE J. Sel. Areas Commun.*, vol. 26, no. 9, pp. 1638–1649, Dec. 2008.
- [7] F. Wu, K. Yang, F. Tong, and T. Tian, "Compressed sensing of delay and doppler spreading in underwater acoustic channels," *IEEE Access*, vol. 6, pp. 36031–36038, 2018.
- [8] B. Li, S. Zhou, M. Stojanovic, L. Freitag, and P. Willett, "Multicarrier communication over underwater acoustic channels with nonuniform doppler shifts," *IEEE J. Ocean. Eng.*, vol. 33, no. 2, pp. 198–209, Apr. 2008.

- [9] J. A. Tropp and A. C. Gilbert, "Signal recovery from random measurements via orthogonal matching pursuit," *IEEE Trans. Inf. Theory*, vol. 53, no. 12, pp. 4655–4666, Dec. 2007.
- [10] L. Wan, X. Qiang, L. Ma, Q. Song, and G. Qiao, "Accurate and efficient path delay estimation in OMP based sparse channel estimation for OFDM with equispaced pilots," *IEEE Wireless Commun. Lett.*, vol. 8, no. 8, pp. 117–120, Feb. 2019.
- [11] A. Beck and M. Teboulle, "Fast gradient-based algorithms for constrained total variation image denoising and deblurring problems," *IEEE Trans. Image Process.*, vol. 18, no. 11, pp. 2419–2434, Nov. 2009.
- [12] M. T. Altabbaa and E. Panayirci, "Channel estimation and equalization algorithm for OFDM-based underwater acoustic communications systems," in *Proc. 13th Int. Conf. Wireless Mobile Commun.*, 2017, pp. 113–118.
- [13] E. Panayirci, M. T. Altabbaa, M. Uysal, and H. V. Poor, "Sparse channel estimation for OFDM-based underwater acoustic systems in rician fading with a new OMP-MAP algorithm," *IEEE Trans. Signal Process.*, vol. 67, no. 6, pp. 1550–1565, Mar. 2019.
- [14] E. Panayirci, H. Senol, M. Uysal, and H. V. Poor, "Sparse channel estimation and equalization for OFDM-based underwater cooperative systems with amplify-and-forward relaying," *IEEE Trans. Signal Process.*, vol. 64, no. 1, pp. 214–228, Sep. 2016.
- [15] M. T. Altabbaa, A. S. Ogrenici, E. Panayirci, and H. V. Poor, "Sparse channel estimation for space-time block coded OFDM-based underwater acoustic channels," in *Proc. IEEE Glob. Commun. Conf.*, 2018, pp. 1–6.
- [16] B. Li and M. Stojanovic, "Alamouti space time coded OFDM for underwater acoustic channels," in *Proc. IEEE OCEANS*, 2010, pp. 1–3.
- [17] R. Roy and T. Kailath, "ESPRIT-estimation of signal parameters via rotational invariance techniques," *IEEE Trans. Acoust., Speech, Signal Process.*, vol. 37, no. 7, pp. 984–995, Jul. 1989.
- [18] H. Eghbali, M. Stojanovic, and S. Muhaidat, "Differential decoding for SFBC OFDM systems in underwater MIMO channels," in *Proc. IEEE Int. Conf. Acous., Speech Signal Process.*, 2014, pp. 8102–8105.
- [19] E. V. Zorita and M. Stojanovic, "Space-frequency block coding for underwater acoustic communications," *IEEE J. Ocean. Eng.*, vol. 40, no. 2, pp. 303–314, Oct. 2015.
- [20] O. Bar-Ilan and Y. C. Eldar, "Sub-nyquist radar via doppler focusing," *IEEE Trans. Signal Process.*, vol. 62, no. 7, pp. 1796–1811, Apr. 2014.
- [21] S. M. Alamouti, "A simple transmit diversity technique for wireless communications," *IEEE J. Sel. Areas Commun.*, vol. 16, no. 8, pp. 1451–1458, Oct. 1998.
- [22] C. R. Berger, S. Zhou, J. Preisig, and P. Willett, "Sparse channel estimation for multicarrier underwater acoustic communication: From subspace methods to compressed sensing," *IEEE Trans. Signal Process.*, vol. 58, no. 3, pp. 1708–1721, Mar. 2010.
- [23] P. Qarabaqi and M. Stojanovic, "Statistical characterization and computationally efficient modeling of a class of underwater acoustic communication channels," *IEEE J. Ocean. Eng.*, vol. 38, no. 4, pp. 701–717, Oct. 2013.
- [24] T. Jensenud and S. Ivansson, "Measurements and modeling of effects of out-of-plane reverberation on the power delay profile for underwater acoustic channels," *IEEE J. Ocean. Eng.*, vol. 40, no. 4, pp. 807–821, Oct. 2015.
- [25] F. Hu, Y. Wang, and L. Jin, "Robust MIMO-OFDM design for CMMB systems based on LMMSE channel estimation," in *Proc. IEEE 5th Int. Conf. Electron. Infor. Emerg. Commun.*, 2015, pp. 59–62.
- [26] H. A. Cirpan, E. Panayirci, and H. Dogan, "Nondata-aided channel estimation for OFDM systems with space-frequency transmit diversity," *IEEE Trans. Veh. Technol.*, vol. 55, no. 2, pp. 449–457, Mar. 2006.
- [27] H. Senol, E. Panayirci, and H. V. Poor, "Nondata-aided joint channel estimation and equalization for OFDM systems in very rapidly varying mobile channels," *IEEE Trans. Signal Process.*, vol. 60, no. 8, pp. 4236–4253, Aug. 2012.
- [28] M. Porter, "Bellhop Gaussian beam/finite element beam code," [Online]. Available: <http://oalib.hlsresearch.com>
- [29] J. C. Peterson and M. B. Porter, "Virtual Timeseries EXperiment (VirTEX)," 2011, [Online]. Available: <http://oalib-acoustic.org>
- [30] J. Llor and M. P. Malumbres, "Statistical modeling of large-scale signal path loss in underwater acoustic networks," *Sensors (Basel)*, vol. 13, no. 2, pp. 2279–2294, 2013.



Erdal Panayirci (Life Fellow, IEEE) received the Dipl. Eng. degree in electrical engineering from Istanbul Technical University, Istanbul, Turkey, in 1964, and the Ph.D. degree in electrical engineering and system science from Michigan State University, East Lansing, MI, USA, in 1971. He is currently a Professor with the Electrical and Electronics Engineering Department, Kadir Has University, Istanbul, Turkey and a Visiting Research Collaborator with the Department of Electrical Engineering, Princeton University, Princeton, NJ, USA. From 2008 to 2009 and from 2017 to 2018, he was with the Department of Electrical Engineering, Princeton University. He has authored or coauthored extensively in leading scientific journals and international conference and coauthored the book *Principles of Integrated Maritime Surveillance Systems* (Kluwer Academic, 2000). His research interests include communication theory, synchronization, and advanced signal processing techniques and their applications to wireless electrical, underwater, and optical communications.

From 1995 to 2000, he was the Editor of the IEEE TRANSACTIONS ON COMMUNICATIONS in the areas of synchronization and equalization. From 2005 to 2008, and from 2018 to 2020, he was a Member of the IEEE Fellow Committee and from 2017 to 2020, a Member of the IEEE GLOBECOM/ICC Management and Strategy Standing Committee. He was the Technical Program Co-Chair of the IEEE International Conference on Communications (ICC2006) and the Technical Program Chair of the IEEE PIMRC, both held in Istanbul in 2006 and 2010, respectively. He was the Executive Vice Chairman of the IEEE Wireless Communications and Networking Conference, Istanbul, Turkey, in April 2014 and the General Co-Chair of the IEEE PIMRC held in Istanbul, Turkey, in September 2019.



Mhd Tahssin Altabbaa (Member, IEEE) received the B.Sc. degree from the Department of Informatics and Communication Engineering, Arab International University, Damascus, Syria, in 2012, and the M.Sc. and Ph.D. degrees in electronics engineering from Kadir Has University, Istanbul, Turkey, in 2015 and 2018, respectively. He is currently an Assistant Professor with Yeni Yüzyıl University, Istanbul, Turkey. His research interests include signal processing for underwater acoustic communications, channel estimation, index modulation, and cognitive radio

networks.



H. Vincent Poor (Life Fellow, IEEE) received the Ph.D. degree in EECS from Princeton University, Princeton, NJ, USA, in 1977. From 1977 to 1990, he was on the faculty of the University of Illinois at Urbana-Champaign, Urbana, IL, USA. Since 1990, he has been on the faculty at Princeton, where he is currently the Michael Henry Strater University Professor of Electrical Engineering. From 2006 to 2016, he was the Dean of Princeton's School of Engineering and Applied Science. He has also held visiting appointments with several other universities, including most recently at Berkeley and Cambridge. His research interests include information theory, machine learning, and networks science, and their applications in wireless networks, energy systems, and related fields. Among his publications in these areas is the forthcoming book *Machine Learning and Wireless Communications*. (Cambridge University Press, 2021).

Dr. Poor is a Member of the National Academy of Engineering and the National Academy of Sciences, and is a Foreign Member of the Chinese Academy of Sciences, the Royal Society, and other national and international academies. Recent recognition of his work includes the 2017 IEEE Alexander Graham Bell Medal, the 2019 ASEE Benjamin Garver Lamme Award, a D.Sc. *honoris causa* from Syracuse University awarded in 2017, and a D.Eng. *honoris causa* from the University of Waterloo awarded in 2019. Since 2018, he has been a Distinguished Lecturer for the IEEE Vehicular Technology Society.